



Master's thesis
Particle Physics and Astrophysical Sciences
Cosmology

Primordial black holes and gravitational waves from inflation

Johannes Halkoaho

October 28, 2022

Supervisor(s): Syksy Räsänen

Examiner(s): Syksy Räsänen
Mark Hindmarsh

UNIVERSITY OF HELSINKI
FACULTY OF SCIENCE

PL 64 (Gustaf Hällströmin katu 2a)
00014 Helsingin yliopisto

Tiedekunta — Fakultet — Faculty Faculty of Science	Koulutusohjelma — Utbildningsprogram — Degree programme Particle Physics and Astrophysical Sciences Cosmology
Tekijä — Författare — Author Johannes Halkoaho	
Työn nimi — Arbetets titel — Title Primordial black holes and gravitational waves from inflation	
Työn laji — Arbetets art — Level Master's thesis	Aika — Datum — Month and year October 28, 2022
Sivumäärä — Sidantal — Number of pages 47	
Tiivistelmä — Referat — Abstract The primordial perturbations created by inflation in the early Universe are known to be able to produce significant amount of primordial black holes and gravitational waves with large amplitudes in some inflationary models. Primordial black holes are produced by primordial scalar perturbations and gravitational waves are partly primordial tensor perturbations and partly produced by scalar perturbations.	
In this thesis we review some of the current literature on the subject and discuss a few inflationary models that are capable of producing primordial scalar perturbations large enough to create a significant amount of primordial black holes. The main focus is on ultra-slow roll inflation with a concrete example potential illustrating the dynamics of the scenario followed by a briefer treatment of some of the alternative models.	
We start by explaining the necessary background theory for the understanding of the subject at hand. Then we move on to the inflationary models covered in this thesis.	
After that we explain the production of the primordial black holes and gravitational waves from scalar perturbations. Then we consider primordial black holes as a dark matter candidate and go through the most significant known restrictions on the existence of primordial black holes with different masses. We discuss some of the possible future constraints for the remaining possible mass window for which primordial black holes could explain all of dark matter. We then briefly discuss two planned space-based gravitational wave detectors that may be able to detect gravitational waves created by inflation.	
Avainsanat — Nyckelord — Keywords L ^A T _E X	
Säilytyspaikka — Förvaringsställe — Where deposited	
Muita tietoja — Övriga uppgifter — Additional information	

Tiedekunta — Fakultet — Faculty	Koulutusohjelma — Utbildningsprogram — Degree programme Alkeishiukkasfysiikka ja astrofysikaaliset tieteet Kosmologia			
Matemaattis-luonnontieteellinen tiedekunta				
Tekijä — Författare — Author				
Johannes Halkoaho				
Työn nimi — Arbetets titel — Title				
Primordial black holes and gravitational waves from inflation				
Työn laji — Arbetets art — Level	Aika — Datum — Month and year	Sivumäärä — Sidantal — Number of pages		
Maisterin tutkielma	October 28, 2022	47		
Tiivistelmä — Referat — Abstract				
<p>Varhaisessa universumissa inflaatiosta syntivien primordiaalisien perturbaatioiden tiedetään pystyvän tuottamaan huomattava määrä primordiaalisia mustia aukkoja ja suuriampelisista gravitaatioaltoja joissakin inflaatiomalleissa. Primordiaaliset mustat aukot syntyvät primordiaalisista skalaariperturbaatioista niiden tullessa takaisin Hubble säteen sisälle inflaation jälkeen. Gravitaatioallot ovat osittain primordiaalisia tensoriperturbaatioita ja osittain syntyvät skalaariperturbaatioista.</p>				
<p>Tässä opinnäytetyössä käymme läpi tämänhetkisen kirjallisuuden tilannetta ja käsittelemme muutamia inflaatiomalleja, jotka pystyvät tuottamaan tarpeeksi suuria primordiaalisia skalaariperturbaatioita synnyttääkseen mielenkiintoisen määrän primordiaalisia mustia aukkoja. Päämallina käsittelemme ultra-slow roll inflaation konkreettisen esimerkki potentiaalin kautta, jota seuraa joidenkin vaihtoehtoisten mallien lyhyempi käsiteily.</p>				
<p>Aloitamme selittämällä aiheeseen liittyvän taustateorian. Tämän jälkeen siirrymme käsittelemään opinnäytetyöhön valittuja inflaatiomalleja.</p>				
<p>Sitten selitämme primordiaalisten mustien aukkojen ja gravitaatioalojen syntymekanismin skalaariperturbaatioista. Tämän jälkeen käsittelemme primordiaalisia mustia aukkoja mahdollisena pimeän aineen ehdokkaana ja käymme läpi tärkeimmät eri massaisten mustien aukkojen runsauteen liittyvät rajoitukset. Keskustelemme joistakin mahdollisista tulevaisuuden rajoituksista massaikunalle, jossa primordiaaliset mustat aukot voisivat vielä selittää kaiken pimeän aineen. Käsittelemme sitten lyhyesti kaksi suunniteltua avaruuteen lähetettävää gravitaatioaltoilmaisinta, jotka mahdollisesti pystyvät havaitsemaan inflaatiosta syntyneitä gravitaatioaloja.</p>				
Avainsanat — Nyckelord — Keywords				
L ^A T _E X				
Säilytyspaikka — Förvaringsställe — Where deposited				
Muita tietoja — Övriga uppgifter — Additional information				

Contents

1	Introduction	2
2	Background theory	4
2.1	Background metric and the equations for the evolution of the Universe	4
2.2	Relevant events in the early Universe	5
2.2.1	Baryogenesis	5
2.2.2	Big bang nucleosynthesis	5
2.2.3	Cosmological background radiation	5
2.3	Inflation	6
2.3.1	Cosmological problems	6
2.3.2	Scalar field	8
2.3.3	Slow roll approximation	9
2.3.4	Reheating	11
2.3.5	Cosmological perturbation theory	12
2.3.6	Primordial perturbations	13
2.3.7	Power spectra	13
2.3.8	Perturbations at Hubble exit	14
2.4	Primordial black holes	15
2.4.1	Lifetime of black holes	15
2.5	Gravitational waves	16
2.5.1	Gravitational waves due linear tensor perturbations from quantum fluctuations	16
2.5.2	Information from primordial gravitational waves	16
3	Inflation models	18
3.1	Ultra-slow roll	18
3.1.1	Effect of quantum diffusion	19
3.1.2	Amplitude of the primordial curvature perturbations in USR	20
3.1.3	Growth of the perturbations in USR	21
3.1.4	Example potential	22

3.1.5	Punctuated inflation	24
3.2	Other inflation models	24
3.2.1	Higgs inflation	24
3.2.2	Hybrid waterfall	26
3.2.3	Curvaton	27
4	Formation of PBH and induced gravitational waves from primordial scalar perturbations	29
4.1	Generation of primordial black holes from re-entry	29
4.1.1	Mass of PBH	29
4.1.2	Probability distribution of PBH abundance	30
4.2	Gravitational waves induced by primordial perturbations	31
4.2.1	The metric	31
4.2.2	Induced gravitational waves	32
4.2.3	Relation to PBH mass	33
5	Primordial black holes as a dark matter candidate	34
5.1	Mass scales	34
5.2	Planck mass relics	35
5.3	Observational limitations	36
5.3.1	Microlensing constraints	36
5.3.2	Accretion	37
5.3.3	Discreteness effects or dynamical constraints	37
5.3.4	Evaporation constraints	38
5.3.5	Constraints from the power spectrum	38
5.3.6	Gravitational wave constraints	39
5.3.7	Future constraints for the asteroid mass range	39
5.4	Future gravitational wave detectors	41
5.4.1	LISA	41
5.4.2	DECIGO	41
6	Conclusion	42

1. Introduction

Primordial black holes (PBH) have been a source of interest for the past 50 years since their existence was first proposed by Stephen Hawking [30] and the recent detection of gravitational waves has raised the interest even more. PBHs are of special interest because they are able to form at essentially any mass. Which means that currently they are the only form of black holes that can be significantly affected by Hawking radiation. They are also a possible dark matter candidate that could compose either a part or all of dark matter [10].

Several mechanisms that could create these objects have been suggested. Examples include PBH formation from domain walls [21] or from vacuum bubbles that nucleate during inflation [20] and theories about nucleated cosmic string loops [27]. One of the more interesting mechanisms is PBH formation from primordial perturbations created by a period of inflation in the early Universe. The properties of this period are still very uncertain and many different models have been suggested to explain different cosmological observations. The abundance of PBHs can be used to constrain and develop new inflation models.

The interest in gravitational waves increased drastically after the first detection of gravitational waves created by the merging of a binary black hole pair by the gravitational wave observatory LIGO [1]. The binary black hole pair could have been of primordial origin, but can also be explained by astrophysical processes. Since the first detection, around 90 mergers have been detected. Inflation also creates primordial gravitational waves that could be detected by future gravitational wave detectors such as LISA and DECIGO. Currently there is no direct observational data from inflation. The current observational data is indirect and gained through the cosmic microwave background (CMB) radiation but with the use of these new gravitational wave detectors, we can possibly get direct experimental data about inflation.

This thesis will go over some of the models that can produce PBHs efficiently enough to be interesting with the focus on ultra-slow roll (USR) inflation scenario. Then we will look at the formation of PBHs and induced gravitational waves from primordial scalar perturbations and finally we will go over the most important observational constraints for PBH mass ranges as potential explanations for dark matter.

We use the natural units where $c = 1$ and $\hbar = 1$. We use the reduced Planck mass related to the Newton's gravitational constant as $M_{pl}^2 = \frac{1}{8\pi G}$.

2. Background theory

In this chapter we cover the necessary background information for understanding PBH and gravitational wave formation from inflation. We mostly follow [13, 37].

2.1 Background metric and the equations for the evolution of the Universe

The background metric for a homogeneous, isotropic and expanding universe is the Friedmann-Lemaître-Robertson-Walker (FLRW) metric. We approximate the Universe as flat which is in line with the observational constraints that imply negligible spatial curvature. Thus the background metric is

$$ds^2 = \bar{g}_{\alpha\beta} dx^\alpha dx^\beta = a^2(\tau) (-d\tau^2 + \delta_{ij} dx^i dx^j), \quad (2.1)$$

where the bar refers to a background quantity and τ is the conformal time defined as $d\tau = \frac{dt}{a(t)}$ where t is the cosmic time and a the cosmic scale factor. There are three important equations for describing the evolution of a homogeneous and isotropic universe. Starting with the first Friedmann equation

$$H^2 = \left(\frac{\dot{a}}{a}\right)^2 = \frac{\rho}{3M_{pl}^2} - \frac{K}{a^2}, \quad (2.2)$$

where ρ is the energy density and K describes the spatial curvature. The dot denotes derivative with respect to cosmic time. For the flat case ($K = 0$) (2.2) reduces to

$$H^2 = \frac{\rho}{3M_{pl}^2}. \quad (2.3)$$

Then there is the second Friedmann equation or the acceleration equation

$$\frac{\ddot{a}}{a} = -\frac{1}{6M_{pl}^2}(\rho + 3P), \quad (2.4)$$

where P is the pressure. The third equation is the continuity equation

$$\dot{\rho} + 3H(\rho + P) = 0. \quad (2.5)$$

As two of these three equations are independent (any two of them can be used to derive the last one), a fourth equation is necessary to solve the three unknowns: $a(t)$, $\rho(t)$ and $P(t)$. The fourth equation is the equation of state

$$P = \omega \rho, \quad (2.6)$$

where ω is the equation of state parameter. Which is 0 for matter, $1/3$ for radiation, for the cosmological constant it is -1 and for curvature $-1/3$ (the contribution of curvature doesn't come from an energy density but from the second term in (2.2)). So $\omega < 0$ corresponds to negative pressure and $\omega > 0$ to positive pressure. Matter is pressureless. This fourth equation can be used to solve for the unknowns from the three previous equations. The linear form of $P(\rho)$ is not the most general but in practice it adequately describes the Universe during most of its evolution.

2.2 Relevant events in the early Universe

2.2.1 Baryogenesis

Baryogenesis is the process that has been hypothesized to have taken place during the early Universe to produce baryonic asymmetry as it is still an open question as to why there is more matter than anti-matter.

2.2.2 Big bang nucleosynthesis

Big bang nucleosynthesis (BBN) happened in the early Universe (around 10 s to 20 min after the big bang). It refers to the creation of other nuclei (up to lithium) than the single proton nuclei that existed in the early Universe.

2.2.3 Cosmological background radiation

The CMB is electromagnetic radiation that is a remnant of the time of recombination (the Universe was around the age of 370 000 years [37]). When the Universe was hot and dense enough for electrons and protons to be unbound from each other the Universe was filled with opaque fog of hydrogen plasma so the light could not travel freely. When the Universe expanded and cooled enough for the first atoms to emerge by the binding of electrons to atomic nuclei it became transparent and photons decoupled from the surrounding matter. The photons from that time form the CMB.

2.3 Inflation

Inflation means a period of the Universe when the expansion of the Universe is accelerating (i.e. $\ddot{a} > 0$). This happened in the early Universe when the Universe underwent exponential expansion in a very short amount of time. From the acceleration equation we see that for the expansion of the Universe to accelerate (ie. $\ddot{a} > 0$) we need pressure negative enough such that $\omega < -\frac{1}{3}$.

2.3.1 Cosmological problems

Inflation is able to answer three classic cosmological problems:

- The horizon problem
- The flatness problem
- Unwanted relics

Horizon problem

The horizon problem or the homogeneity problem refers to the homogeneous and isotropic nature of the CMB. This includes the areas of the sky that should not have yet had the time to be in causal contact with each other i.e. regions separated by more than 1° and yet have the same temperature with the accuracy of $\lesssim 10^{-4}$.

Inflation can be discussed in terms of physical distances or in terms of comoving distances. During inflation the physical distance between two points is increasing with an accelerating rate. The benefit of using comoving units is that we can keep the distance between two points fixed in an expanding universe.

The comoving Hubble length , $\frac{1}{\dot{a}} = \mathcal{H}^{-1}$, gives the distance over which we have causal interaction on cosmological timescales in comoving units. During inflation the comoving Hubble length is shrinking. From the comoving viewpoint when \mathcal{H}^{-1} shrinks the comoving distance for which we have causal connection also shrinks and the region causally connected to a given location in the Universe shrinks. From the physical viewpoint the distance between two points is increasing faster than the distance over which causal contact can be had. Which would explain the horizon problem i.e. the regions were causally connected before inflation.

Flatness problem

The flatness problem refers to the fact that the Universe seems to be on average almost perfectly spatially flat. Given the first Friedmann equation in the form

$$\Omega - 1 = \frac{K}{a^2 H^2}, \quad (2.7)$$

where Ω is the density parameter defined as

$$\Omega \equiv \frac{\rho}{\rho_c} = \frac{8\pi G \rho}{3H^2}, \quad (2.8)$$

where ρ_c is the critical density of the Universe. For individual components such as the matter Ω_m or dark matter Ω_{dm} the definition is

$$\Omega_m \equiv \frac{\rho_m}{\rho_c} = \frac{8\pi G \rho_m}{3H^2}, \quad \Omega_{dm} \equiv \frac{\rho_{dm}}{\rho_c} = \frac{8\pi G \rho_{dm}}{3H^2}. \quad (2.9)$$

We see that if the Universe has a critical density $\Omega = 1$, it stays like that since $K=0$.

If the initial value of the density parameter (Ω_i) during the radiation dominated era is not be extremely close to one, one of two things can happen. If Ω_i is significantly greater than 1 then the Universe recollapses in a relatively short time. And if Ω_i is significantly smaller than 1 the expansion of the Universe is dominated by the curvature and the scale factor grows $a \propto t$ compared to radiation and matter domination $a \propto t^{1/2}$ and $a \propto t^{2/3}$ respectively. Neither of these describes the Universe we live in. During inflation

$$|1 - \Omega| = \frac{|K|}{a^2 H^2} \quad (2.10)$$

shrinks. So Ω is driven very close to 1.

Unwanted relics

It is possible that the extremely high temperatures at the beginning of the Universe would allow the formation of stable high energy relics in a significant number. One of such relics is the magnetic monopole that is predicted to be created during the phase transition that could have happened when the electroweak force and the strong force separated. This breakdown of the Grand Unified Force (GUT) into two separate forces is theorized to have happened very early in the Universe around $t \sim 10^{-36}$ s. The GUT energy scale is believed to be around 10^{16} GeV and it is predicted for the magnetic monopoles to have a rest mass of similar magnitude. Due to their high rest mass if magnetic monopoles formed in a significant number, they would come to dominate the energy density today which is clearly not the case.

Inflation solves this by diluting the number of the relics to such densities that they are not a problem. This sets limits on the reheating temperature. Meaning that the reheating temperature has to be low enough that it doesn't generate more of such relics.

2.3.2 Scalar field

Inflation is commonly modeled by being driven by a scalar field called the inflaton. This section goes over the properties of a scalar field, and follows [37]. In the beginning we use the Minkowski metric $\eta = \text{diag}(-1, 1, 1, 1)$ and later generalize to an expanding universe.

Let us start with a single scalar field ϕ with potential given by $V(\phi)$. The Lagrangian of the scalar field is

$$\mathcal{L} = -\frac{1}{2}\partial_\mu\phi\partial^\mu\phi - V(\phi) . \quad (2.11)$$

Now the field equation is obtained from the Lagrangian by minimizing the action [37]

$$\int \mathcal{L} d^4x . \quad (2.12)$$

This leads to the Euler-Lagrange equation

$$\frac{\partial\mathcal{L}}{\partial\phi(x)} - \partial_\mu\frac{\partial\mathcal{L}}{\partial[\partial_\mu\phi(x)]} = 0 . \quad (2.13)$$

For the scalar field this leads to the field equation

$$\partial_\mu\partial^\mu\phi - V'(\phi) = 0 , \quad (2.14)$$

where $\partial_\mu\partial^\mu\phi = -\ddot{\phi} + \nabla^2\phi$, $\nabla^2 = \partial_i\partial^i$ and $V'(\phi) = \frac{dV}{d\phi}$. So the field equation is

$$\ddot{\phi} - \nabla^2\phi = -V'(\phi) . \quad (2.15)$$

The Lagrangian gives the energy momentum tensor as

$$T^{\mu\nu} = \frac{\partial\mathcal{L}}{\partial(\partial_\mu\phi)}\partial^\nu\phi + \eta^{\mu\nu}\mathcal{L} . \quad (2.16)$$

So for the scalar field the energy momentum tensor is

$$T^{\mu\nu} = \partial^\mu\phi\partial^\nu\phi - \eta^{\mu\nu}\left[\frac{1}{2}\partial_\rho\phi\partial^\rho\phi + V(\phi)\right] . \quad (2.17)$$

From this we get the energy density and the pressure of the scalar field as $\rho = T^{00}$ and $p = \frac{1}{3}(T^{11} + T^{22} + T^{33})$. Then these quantities become

$$\rho_\phi = \frac{1}{2}\dot{\phi}^2 + \frac{1}{2}(\nabla\phi)^2 + V(\phi) \quad (2.18)$$

$$P_\phi = \frac{1}{2}\dot{\phi}^2 - \frac{1}{6}(\nabla\phi)^2 - V(\phi) . \quad (2.19)$$

Now moving to the FLRW case. Considering an inflaton field that during inflation is almost homogeneous ($(\nabla\phi)^2 \approx 0$) as is the case in FLRW. The energy density and pressure of this scalar inflaton field become

$$\rho_\phi = \frac{1}{2}\dot{\phi}^2 + V(\phi) \quad (2.20)$$

$$P_\phi = \frac{1}{2}\dot{\phi}^2 - V(\phi) . \quad (2.21)$$

In this case the equation of state parameter is

$$\omega = \frac{\frac{1}{2}\dot{\phi}^2 - V(\phi)}{\frac{1}{2}\dot{\phi}^2 + V(\phi)} . \quad (2.22)$$

Now we need to modify the field equation for an expanding universe which can be done by inserting (2.20) and (2.21) into (2.5)

$$\dot{\rho} + 3H(\rho + P) = \dot{\phi}\ddot{\phi} + V'\dot{\phi} + 3H\left(\frac{1}{2}\dot{\phi}^2 + V(\phi) + \frac{1}{2}\dot{\phi}^2 - V(\phi)\right) = \ddot{\phi} + 3H\dot{\phi} + V' = 0 . \quad (2.23)$$

Equation of motion of the homogeneous inflaton field in an expanding universe is then

$$\ddot{\phi} + 3H\dot{\phi} + V' = 0 . \quad (2.24)$$

The condition for inflation $\ddot{a} > 0$ (or $\rho + 3P = 2\dot{\phi} - 2V(\phi) < 0$) is satisfied when $\dot{\phi}^2 < V(\phi)$. Meaning that the kinetic energy of the field is smaller than the potential energy of the field. And the equation of state parameter will be close to the cosmological constant ($\omega \approx -1$) when $\frac{1}{2}\dot{\phi}^2 \ll V(\phi)$.

Now (2.3) becomes

$$H^2 = \frac{1}{3M_{Pl}^2} \left[\frac{1}{2}\dot{\phi}^2 + V(\phi) \right] , \quad (2.25)$$

where contributions to the energy density from everything else except the inflaton field are ignored. The reason for this is that as the inflaton field moves slowly the energy density dominated by the potential also changes slowly. The matter and radiation components decrease very fast ($\rho_m \propto a^{-3}$ and $\rho_r \propto a^{-4}$) which means that they become quickly negligible during inflation.

Taking the time derivative of (2.25) and inserting the equation of motion (2.24) we can derive the identity

$$\dot{H} = \frac{-\dot{\phi}^2}{2M_{Pl}^2} . \quad (2.26)$$

2.3.3 Slow roll approximation

The friction term ($3H\dot{\phi}$) of the field equation (2.24) slows down the evolution of ϕ . This can lead to the fulfillment of the slow roll (SR) conditions

$$\dot{\phi}^2 \ll V(\phi) \quad (2.27)$$

$$|\ddot{\phi}| \ll |3H\dot{\phi}| . \quad (2.28)$$

With this SR approximation the equations (2.3) and (2.24) reduce to

$$3M_{Pl}^2 H^2 \approx V(\phi) \quad (2.29)$$

$$3H\dot{\phi} \approx -V' . \quad (2.30)$$

Defining the Hubble SR parameters

$$\epsilon_H \equiv -\frac{\dot{H}}{H^2} = \frac{\dot{\phi}^2}{2H^2 M_{Pl}^2} \quad (2.31)$$

$$\eta_H \equiv \frac{\dot{\epsilon}_H}{H\epsilon_H} \approx \frac{\frac{d\epsilon_H}{d\Delta N}}{\epsilon_H} . \quad (2.32)$$

The parameter ϵ_H measures the ratio of the kinetic energy density to the total energy density and η_H measures how quickly ϵ_H varies with time. Assuming the potential energy dominates $\epsilon_H \ll 1$. Two other parameters defined using the potential instead are

$$\epsilon_V \equiv \frac{M_{Pl}^2}{2} \left(\frac{V'}{V} \right)^2 \quad (2.33)$$

$$\eta_V \equiv M_{Pl}^2 \frac{V''}{V} . \quad (2.34)$$

In SR the conditions imply that

$$\epsilon_H \approx \epsilon_V \ll 1, |\eta_H| \approx |\eta_V| \ll 1 . \quad (2.35)$$

The conditions for the potential SR parameters are necessary conditions for the SR approximation to be valid and for inflation to occur but not sufficient ones. They only constrain the shape of the potential [37]. Here we will use primarily the Hubble SR parameters as they contain the necessary information and are sufficient conditions for inflation with the true end point being $\epsilon_H = 1$ while with the potential SR parameter the inflation ending at $\epsilon_V = 1$ is only a first order result [39]. Now we will write condition for inflation using ϵ_H starting with the definition of the Hubble parameter

$$H = \frac{\dot{a}}{a}, \dot{H} = \frac{\ddot{a}}{a} - \frac{\dot{a}^2}{a^2} \quad (2.36)$$

$$\frac{\ddot{a}}{a} = \dot{H} + H^2 . \quad (2.37)$$

And given that $a > 0$ the inflation condition $\ddot{a} > 0$ becomes

$$\dot{H} + H^2 > 0 . \quad (2.38)$$

Using (2.3) and (2.4) we see that [37]

$$\dot{H} = \frac{\ddot{a}}{a} - \frac{\dot{a}^2}{a^2} = -\frac{1}{6M_{Pl}^2}(\rho + 3P) - \frac{\rho}{3M_{Pl}^2} = -\frac{1}{6M_{Pl}^2}(\rho + p) . \quad (2.39)$$

This would mean that for $\dot{H} > 0$ it would be that $p < -\rho$ meaning $\omega < -1$ which is not allowed by the equations (2.20) and (2.21). So it has to be that $\dot{H} \leq 0$. The inflation condition can then be written as

$$-\frac{\dot{H}}{H^2} = \epsilon_H < 1 . \quad (2.40)$$

So if the Hubble SR conditions apply inflation is guaranteed. The above can also be written in the form

$$\left| \frac{\dot{H}}{H} \right| \ll \frac{\dot{a}}{a} \quad (2.41)$$

The Hubble parameter changes much more slowly than the scale factor and for a constant Hubble parameter the Universe expands exponentially. This expansion is measured in e-folds meaning that how many orders in e the Universe has expanded.

Number of e-foldings from time t to end of inflation t_{end} is given by the definition

$$N(t) \equiv \ln \frac{a(t_{end})}{a(t)} , \quad (2.42)$$

this using $d \ln a = \frac{da}{a} = H dt = H \frac{d\phi}{\dot{\phi}}$ and the SR equations (2.29) and (2.30) can be put in the form

$$N(\phi) = \int_t^{t_{end}} H(t) dt = \int_{\phi}^{\phi_{end}} \frac{H}{\dot{\phi}} d\phi \approx \frac{1}{M_{Pl}^2} \int_{\phi}^{\phi_{end}} \frac{V}{V'} d\phi , \quad (2.43)$$

where in the last step we have used the SR approximation. To solve the horizon and flatness problems the amount of e-foldings is assumed to be around 50-60.

2.3.4 Reheating

During inflation most of the energy is in the inflaton potential as is seen from the SR condition $\dot{\phi}^2 \ll V(\phi)$. When inflation ends, the potential of the inflaton field decays into standard model (SM) particles and the energy is transferred to a thermal bath of particles in the reheating process. Thus from the potential $V(\phi)$ reheating creates the matter and radiation seen in the later Universe. It is not clear whether the Universe was ever in thermal equilibrium before inflation so the term reheating might be inaccurate.

Reheating temperature must be high enough for BBN to occur after reheating but sufficiently low that we do not produce any undiluted unwanted relics which depends on the model but should be less than the GUT scale. Then the reheating temperature is at the very least between

$$1 \text{ MeV} < T_{reh} < 10^{16} \text{ GeV} .$$

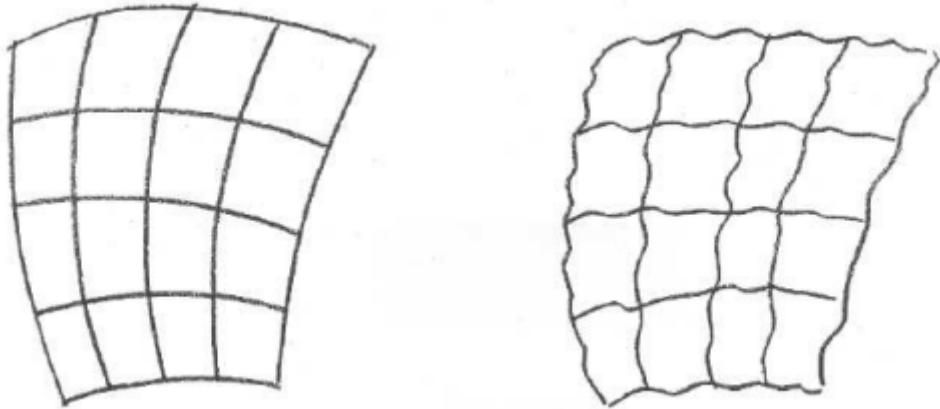


Figure 2.1: This figure shows the difference between the background spacetime and the perturbed spacetime with the simple background spacetime on the left and the perturbed spacetime on the right. Figure taken from [36].

2.3.5 Cosmological perturbation theory

The cosmological perturbation theory is a theory of perturbed spacetime [36]. The perturbed spacetime is very close to the simple background spacetime but as the name suggests is slightly perturbed. In the case of cosmological perturbation theory the background is the FLRW background. The difference between the background spacetime and the perturbed one is illustrated in figure 2.1. This means that there exists a coordinate system where the metric can be written as

$$g_{\alpha\beta} = \bar{g}_{\alpha\beta} + \delta g_{\alpha\beta} , \quad (2.44)$$

where $g_{\alpha\beta}$ is the perturbed metric, $\bar{g}_{\alpha\beta}$ is the FLRW background and $\delta g_{\alpha\beta}$ is a small perturbation. It is also required that the first partial derivatives of the perturbation $\delta g_{\alpha\beta}$ are small and usually second partial derivatives are small as well.

Perturbation theory can be divided into different orders. In first order or linear perturbation theory the products of the small quantities are all dropped and at the second order one keeps the products of two small quantities etc..

The metric perturbation can be divided into three parts based on transform properties under rotations in the background space, a scalar, a vector and a tensor part [36]. In the first order perturbation theory the scalar, vector and tensor parts do not couple to each other, meaning that they evolve independently in time. At second order this is not the case and one of the consequences of this will be explored later.

The scalar perturbations are the most important as they couple to density and pressure perturbations and exhibit gravitational instability as overdense regions grow

more overdense. Vector perturbations couple to rotational velocity perturbations in the cosmic fluid and decay in an expanding universe. Thus they are most likely not important for inflation. Tensor perturbation are gravitational waves. If the waves are strong enough they can have an observable effect on the anisotropy of the CMB.

2.3.6 Primordial perturbations

Most of current inflation research is not focused on it's ability to solve the problems mentioned before but due to it's ability to create primordial perturbations that created the large scale structures we see today. The perturbations can also be a source of PBHs and gravitational waves. PBHs are caused by scalar perturbations at first order [13]. Primordial gravitational waves are primordial tensor perturbations [52] at first order and generated by scalar perturbations at second order [7].

2.3.7 Power spectra

The power spectra of the scalar field perturbations (denoted as $\delta\phi$) and tensor (denoted as h) perturbations are given by [13]

$$\mathcal{P}_{\phi,*} = \left(\frac{H_*}{2\pi} \right)^2 \quad (2.45)$$

$$\mathcal{P}_{T,*} = \frac{8}{M_{pl}} \left(\frac{H_*}{2\pi} \right)^2. \quad (2.46)$$

The * means that the quantity is evaluated at the Hubble crossing ($k=aH$) which we will drop after this. It is useful to consider the comoving curvature perturbation written as

$$\mathcal{R} = \frac{H}{\dot{\phi}} \delta\phi = \frac{\delta\phi}{M_{pl} \sqrt{2\epsilon_H}}. \quad (2.47)$$

The power spectrum of this quantity measured at the Hubble crossing of a specific scale is given by

$$\mathcal{P}_R = \frac{1}{2M_{pl}^2 \epsilon_H} \left(\frac{H}{2\pi} \right)^2. \quad (2.48)$$

The main source of observational data for the curvature perturbation is the CMB observations from which we gain information about the anisotropies of temperature and polarization of the CMB that are effected by the curvature perturbations. The other observational source of data is the matter distribution in the Universe.

The statistical properties of the primordial power spectrum that are deduced from the CMB maps can be parameterised in terms of the power spectrum with two free parameters [13]

$$\mathcal{P}_{\mathcal{R}} = A_s \left(\frac{k}{k_{\text{pivot}}} \right)^{n_s-1}, \quad (2.49)$$

where A_s is the amplitude of the primordial power spectrum, $n_s - 1$ is the spectral index and k_{pivot} is a chosen normalization scale. For a spectral index at the leading order in SR we have

$$n_s - 1 = -6\epsilon_H + 2\eta_H . \quad (2.50)$$

From which we can in SR tell the scale dependence of the primordial power spectrum in terms of the derivatives of the potential with respect to the scalar field as $\epsilon_H \approx \epsilon_V$ and $\eta_H \approx \eta_V$.

The amplitude of the primordial tensor perturbations can be presented as a ratio compared to the amplitude of the scalar perturbations i.e. tensor-to-scalar ratio

$$r \equiv \frac{\mathcal{P}_T}{\mathcal{P}_R} = 16\epsilon_H . \quad (2.51)$$

From the Planck satellite we have the constraints on the spectral index and the tensor-to-scalar ratio as [46]

$$n_s - 1 = 0.965 \pm 0.004$$

$$r \leq 0.1 .$$

Combining the Planck data with the ground-based data from BICEP-Keck strengthens the constraint for r to be $r < 0.032$ [57].

2.3.8 Perturbations at Hubble exit

The curvature perturbations in SR freeze out at the Hubble exit ($k = aH$). Meaning that the perturbations stop evolving in time.

The equation of motion of the curvature perturbation written in terms of τ is

$$\frac{\partial^2 \mathcal{R}_k}{\partial \tau^2} + \frac{2}{z} \frac{\partial z}{\partial \tau} \frac{\partial \mathcal{R}_k}{\partial \tau} + k^2 \mathcal{R}_k = 0 , \quad (2.52)$$

with $z^2 = 2a^2 M_{pl}^2 \epsilon_H$. Given the limit $k \ll aH$ one can find a partially analytic solution by dropping the last term. The solution depends on two k dependent constants C_k and D_k that in turn depend on the initial conditions

$$\mathcal{R}_{k \rightarrow 0} = C_k + D_k \int^{\tau} \frac{d\tau'}{a^2 \epsilon_H} = C_k + D_k \int^t \frac{dt'}{a^3 \epsilon_H} , \quad (2.53)$$

where the constant C_k corresponds to the mode that left the Hubble during SR and remains constant after the Hubble exit. D_k corresponds to the decaying mode. During SR ϵ_H is roughly constant and the decaying mode decays in proportion to a^{-3} . This means that \mathcal{R}_k approaches a constant value due to the decay of the last term.

2.4 Primordial black holes

Normal or stellar black holes can form when a star reaches the end of its life and is left with sufficient mass to initiate a gravitational collapse creating a density high enough for a black hole to form. The maximum mass for a stable white dwarf star is called the Chandrasekhar limit ($1.4 M_{\odot}$) and for a neutron star it is the Tolman-Oppenheimer-Volkoff (TOV) limit which is more difficult to estimate but is thought to be around $2 - 3M_{\odot}$. The stars that have remnants above the TOV limit collapse into black holes.

PBHs are black holes that form at the early times of the Universe and via a different mechanism than stellar black holes. Unlike the stellar black holes, PBHs can be born with a mass less than the Chandrasekhar limit. The highly compressed matter/radiation present in the early Universe allows the formation of black holes with a wide variety of masses from stellar/super-massive scales to the the Planck mass scale [53].

The most studied formation mechanism and the one that is related to this thesis is the formation of PBHs from the gravitational collapse of over-dense regions in the early Universe. The over-densities are created by the scalar primordial perturbations and collapse happens when the modes of those perturbations re-enter the Hubble radius.

For an inflationary model to be a viable candidate for the formation of PBH one has to simultaneously realize the large amplitude fluctuations at small scales so that PBH can form and fit the observational data i.e. amplitude on the CMB scales for the primordial curvature perturbations [53].

2.4.1 Lifetime of black holes

It is theorized that black holes radiate energy through a process called Hawking radiation. The radiation is blackbody radiation with a temperature that scales as

$$T \propto M_{PBH}^{-1}. \quad (2.54)$$

Blackbody radiation is proportional to the surface area of the black hole A as T^4/A , with $A \propto M_{PBH}^2$. Thus the total energy radiated away is proportional to $T^4 A \propto M_{PBH}^{-2}$ and the rate of total energy loss satisfies

$$\frac{dM_{PBH}}{dt} \propto \frac{1}{M_{PBH}^2}, \quad (2.55)$$

which can be easily integrated to

$$t \propto M_{PBH}^3. \quad (2.56)$$

PBHs with initial mass of around $M_{PBH} < M_* \approx 5 \times 10^{14} g$ have already evaporated during the lifetime of the Universe. It is unclear whether black holes evaporate completely or leave behind relics with Planck mass [35].

2.5 Gravitational waves

Gravitational waves give a unique opportunity to probe the earliest times of the Universe due to them not being strongly affected by surrounding matter. While we can use electromagnetic radiation to directly see only the time after recombination, gravitational waves could be a window to the earliest times of the Universe and can be used to probe the mechanics of inflation using future gravitational wave observatories LISA [9] and DECIGO [34]. Currently the only direct observations of gravitational waves are from binary mergers. While the upper limit for the tensor-to-scalar ratio is inferred from the CMB observations. The tensor-to-scalar ratio only concerns the primordial tensor perturbations.

2.5.1 Gravitational waves due linear tensor perturbations from quantum fluctuations

At first order the gravitational waves from inflation are the quantum tensor fluctuations of the metric and are often called primordial gravitational waves. This contributes to the stochastic background of gravitational waves that would be detected by a detector that is sensitive in the proper range. The stochastic background of gravitational waves consists of the superposition of numerous incoherent sources [16]. The stochastic background includes both cosmological sources and astrophysical sources and is considered to be isotropic analogous to the CMB. An example of a astrophysical source would be mergers that can't be individually resolved by the detectors.

2.5.2 Information from primordial gravitational waves

Primordial gravitational waves can be used to constrain different aspects of the early Universe and the possible underlying fundamental physics theory. Here we will give two examples of the constraints.

One of the constraints comes from the relation of the tensor-to-scalar ratio to the energy scale of SR inflation at the time the pivot scale leaves the Hubble radius. Given that during SR inflation the equation (2.29) applies and the power spectrum has the relations (2.48) and (2.49) then at the pivot scale

$$V = 24\pi^2 M_{pl}^4 A_s \epsilon_H . \quad (2.57)$$

With (2.51) and given the scalar amplitude given by Planck Collaboration the energy scale becomes [29]

$$V = (1.88 \times 10^{16} \text{GeV})^4 \frac{r}{0.1} , \quad (2.58)$$

thus r provides the energy scale for inflation.

Another constraint concerns the variation of the inflaton field expectation value from the Hubble crossing of large-scale perturbations to the end of inflation. Given the relation (2.51) and (2.31) we can express r in the form

$$r = \frac{8\dot{\phi}^2}{H^2 M_{Pl}^2} = \frac{8}{M_{Pl}^2} \left(\frac{d\phi}{dN} \right)^2. \quad (2.59)$$

Integrating this from the Hubble crossing of the pivot scale to the end of inflaton and making the dependence of r on N explicit we get

$$\frac{\Delta\phi}{M_{pl}} = \left(\frac{r(\phi_c)}{8} \right)^{1/2} \int_{N_{\phi_c}}^{N_{\phi_{end}}} \left(\frac{r(N)}{r(\phi_c)} \right)^{1/2} dN, \quad (2.60)$$

where ϕ_c is the value at the crossing of the pivot scale. The integral can be considered to be the effective number of e-foldings (N_e) that takes into account the variation of r [29] so we get

$$\frac{\Delta\phi}{M_{pl}} = \left(\frac{r(\phi_c)}{8} \right)^{1/2} N_e. \quad (2.61)$$

The value of N_e is model dependent as it depends on the evolution of r during inflation. For SR inflation r is constant at first-order so N_e becomes just the number of e-foldings. Keeping the SR approximation that is in agreement with the chosen pivot scale we get a lower bound for the deviation. Using the value of for example $N_e \simeq 30$ (i.e. a comoving scale leaving the Hubble radius 30 e-folds before the end of inflation) we get [29]

$$\frac{\Delta\phi}{M_{pl}} \gtrsim 1.06 \left(\frac{r(\phi_c)}{0.01} \right)^{1/2}. \quad (2.62)$$

This means that a model that produces a large number of GW involves a field deviation of the order of Planck mass. This can be used to classify inflationary models into small field and large field models with the distinguishing value being the Planck mass i.e. $\frac{\Delta\phi}{M_{pl}} < 1$ and $\frac{\Delta\phi}{M_{pl}} > 1$.

3. Inflation models

Models of inflation consist of two things: a potential $V(\phi)$ and a way of ending inflation. Broadly there are two ways of ending the inflation. The first one is that the SR approximation is no longer valid when ϕ approaches the minimum of the potential $V(\phi_{min}) \approx 0$. Inflation ends when $\epsilon_H = 1$, the value of ϕ at this time is denoted as ϕ_{end} . The second is that some extra physics intervene with the process to end inflation. As an example of this later is the hybrid waterfall inflation for which the potential is dependant on two different fields. In this case the inflation may end before the SR approximation becomes invalid [37].

The background pressure at the time of the radiation domination was large $P = \omega\rho = \frac{1}{3}\rho$. This means that only large perturbations in the matter density are able to overcome the pressure and collapse into a black hole. Typical amplitude of density perturbations on the CMB scales is $\delta \sim \sqrt{A_s} \sim 5 \times 10^{-5}$ [13] which is too small for PBH production. It is required for δ to be comparable to unity. We know that on the CMB scales the spectral index satisfies $n_s - 1 \approx 0$. If the perturbations are scale invariant or they are smaller on smaller scales then there will not form a significant amount of PBHs at any mass scale. In order for an inflation model to produce PBHs a spike in the primordial curvature perturbation spectrum on small scales is needed without disturbing the power spectrum of the CMB scale.

There exists multiple different models for inflation that are capable producing this. Some are of the single field variety in which only one field is responsible for inflation and the formation of PBH but there are some models that use multiple fields. This review focuses on the USR inflation case more in depth and gives a couple other examples in less detail.

3.1 Ultra-slow roll

In USR $V'(\phi) \approx 0$ [13]. Recalling that the equation of motion for the inflaton field is (2.24) and that the energy density of the Universe is dominated by the potential energy of the field then $V'(\phi) \approx 0$ would give rise to eternal inflation in the SR approximation ($\ddot{\phi} \approx 0$) as the field would not be rolling at all i.e. $\dot{\phi} = 0$. But we can no longer neglect

the acceleration term ($\ddot{\phi}$) due to its smallness and the equation of motion becomes

$$\ddot{\phi} + 3H\dot{\phi} = 0, \quad (3.1)$$

which is the equation of motion for the USR inflation. This means that USR is a separate inflation scenario from SR with opposite approximations. Now solving (3.1) with $v = \dot{\phi}$ and $H = \frac{\dot{a}}{a}$.

$$\dot{v} = -3v\frac{\dot{a}}{a}. \quad (3.2)$$

We see that $v = \dot{\phi} \propto a^{-3}$. Remembering (2.31) with $\dot{\phi} \propto a^{-3}$ then $\epsilon_H \propto a^{-6} \propto e^{-6Ht} \propto e^{-6\Delta N}$, where the fact that $\Delta N \approx Ht$ was used. Then (2.32) gives the result that $\eta_H \approx -6$ during USR as opposed to the SR case where $|\eta_H| \approx |\eta_V| \ll 1$.

Often an inflationary model that has USR as the method for causing a spike in the spectrum consists of the regular SR stage and a USR phase lasting multiple e-foldings. A general form of a typical potential is shown in figure 3.1. In the specific example potential used in this thesis the transition to USR happens in a (near) inflection point of the potential i.e. when $V'' \approx 0$.

The transition between SR and USR can be understood as follows [23]. When the slope ($|V'|$) starts reducing drastically during SR, the friction term ($3H\dot{\phi}$) at first drags along with the slope as they are connected via (2.30) decreasing the value of $|\dot{\phi}|$ and the kinetic energy density $\rho_k = \frac{1}{2}\dot{\phi}^2$. The kinetic energy density decreases faster than normally allowed in SR (i.e. $\max \rho_k \propto a^{-6}$) by the decreasing of the slope. This causes the system to break away from SR. Eventually as the slope drags down the friction term it becomes comparable with the acceleration term ($\ddot{\phi}$). When the terms are comparable the friction term becomes locked with the acceleration term which leads to USR.

3.1.1 Effect of quantum diffusion

If the potential is extremely flat (i.e. has an inflection point) quantum fluctuations of the field may start to dominate its variation [23]. When the potential starts becoming flat the classic motion ($\dot{\phi}$) slows down due to the equation (2.30) and as it slows down enough the significance of the quantum fluctuations increase. The quantum variation of the field per Hubble time $\delta t = H^{-1}$ is usually given by the Hawking temperature in de Sitter space $\delta\phi = \frac{H}{2\pi}$. This gives the kinetic energy density of the quantum fluctuations as [23]

$$\rho_k^{diff} = \frac{1}{2} \left(\frac{\delta\phi}{\delta t} \right)^2 = \frac{H^4}{8\pi^4}, \quad (3.3)$$

which can be interpreted as the minimum value the kinetic density can have. Now assuming $|V'| < \frac{3}{2\pi}H^3$ (i.e. $|\dot{\phi}| = \frac{|V'|}{3H} < \frac{H^2}{2\pi} = \frac{\delta\phi}{\delta t}$) the quantum fluctuations overwhelm SR

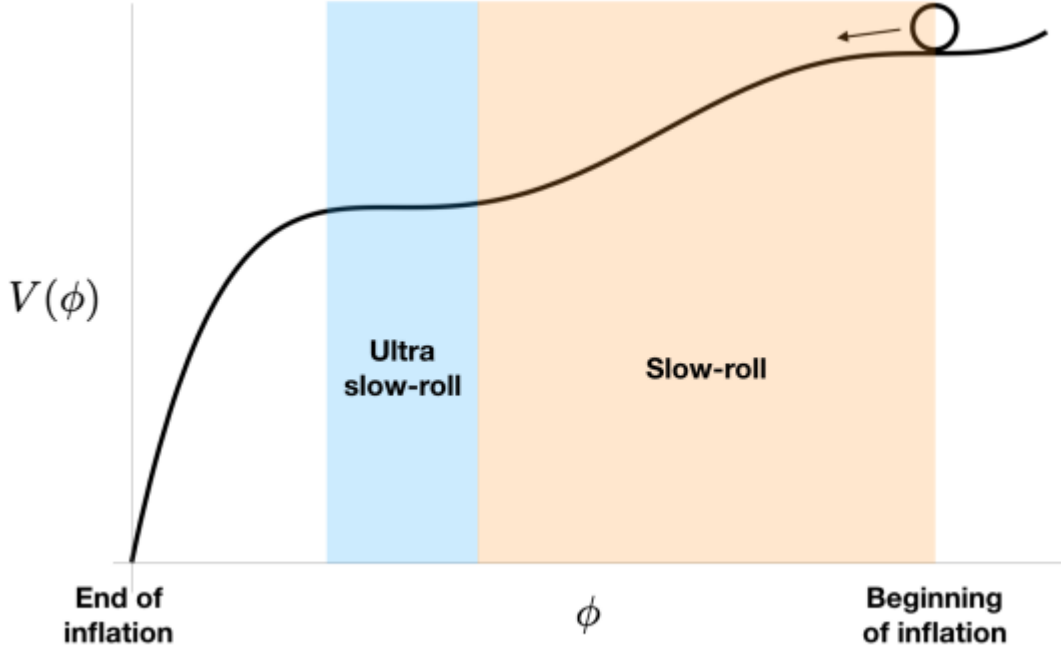


Figure 3.1: An example of the shape of a potential with a USR section and a SR section is shown in this figure. Figure is taken from [18].

so that the number of USR e-folds is [23]

$$\Delta N_{USR} = \frac{1}{6} \ln \frac{\rho_k^0}{\rho_k^{diff}} = \frac{1}{3} \ln \left(6\pi \frac{\sqrt{2\rho_k^0 M_{pl}}}{V} \right), \quad (3.4)$$

3.1.2 Amplitude of the primordial curvature perturbations in USR

In single-field SR inflation the power spectrum can be put in a form using the SR parameter ϵ_H [13]

$$\mathcal{P}_{\mathcal{R}}(k) = \frac{H^2}{8\pi^2 M_{pl}^2 \epsilon_H}. \quad (3.5)$$

This appears to remain at least partially true when USR inflation occurs. It is not true for all scales and is subject to some more details [13].

In USR the perturbations do not freeze out at the Hubble exit, meaning that the formula will have to be evaluated at the time USR ends and not at the Hubble exit. In SR the parameters ϵ_V and ϵ_H are approximately equal to each other. In USR however as $V' \approx 0$ then $\epsilon_V \approx 0 \neq \epsilon_H$ so the parameters can't be treated as interchangeable. Meaning that the formula of the power spectrum has to be evaluated using ϵ_H . Remembering that

$\epsilon_H \propto a^{-6}$ in USR we can see that

$$\mathcal{P}_{\mathcal{R}} \propto e^{6\Delta N}. \quad (3.6)$$

This means that the primordial curvature perturbation grows exponentially (on some scales) during USR inflation creating the spike on the spectrum needed for PBH formation.

This also means that USR cannot last for too many e-folds as that would mean that $\mathcal{P}_{\mathcal{R}} \rightarrow 1$. This signifies the breakdown of perturbation theory as the perturbations are no longer small and would also cause eternal inflation due to [13]

$$\sqrt{\mathcal{P}_{\mathcal{R}}} \sim \frac{H}{\epsilon} \sim \frac{H}{\frac{\Delta\phi}{\Delta N}} \sim 1. \quad (3.7)$$

Meaning that the quantum fluctuations of the field which as we remember have an amplitude of $\delta\phi = \frac{H}{2\pi}$ are of the same magnitude as the distance the inflaton field will roll down the potential during 1 e-fold of inflation at the background level ($\Delta\phi \sim H\Delta N$). This means that it is as likely for the field to quantum leap up the potential as it is for it to continue moving towards the minimum of the potential preventing the inflation from ending in all locations.

3.1.3 Growth of the perturbations in USR

Scalar perturbations

Now to look at how the solution (2.53) behaves during USR. We can now see that the decaying term (despite the name) does not decay as ϵ is no longer close to constant but is proportional to a^{-6} . This leads to [13]

$$\mathcal{R}_k \propto D_k \int^t dt' a^3 \propto \int^t dt' e^{3Ht'} \propto e^{3Ht} \propto a^3, \quad (3.8)$$

as $a \propto e^{Ht}$ during inflation. Hence the curvature perturbations during USR have the same time dependence after Hubble crossing as before [13]

$$\mathcal{P}_{\mathcal{R}}^{USR} \sim \mathcal{R}_k^2 \propto a^6 \quad (3.9)$$

instead of freezing out as in SR.

Tensor perturbations

The equation of motion of the tensor perturbations (h_{ij}) in vacuum is [52]*

$$h_{ij}'' + 2\mathcal{H}h_{ij}' + k^2 h_{ij} = 0, \quad (3.10)$$

where in this case the prime denotes a derivative with respect to τ . This holds both in SR and USR and thus the tensor power spectrum is not amplified during USR and can be written with the standard result (2.46) [50].

*There is a typo in [52] in equation (2.8) with the h_{ij} replaced with h'_{ij}

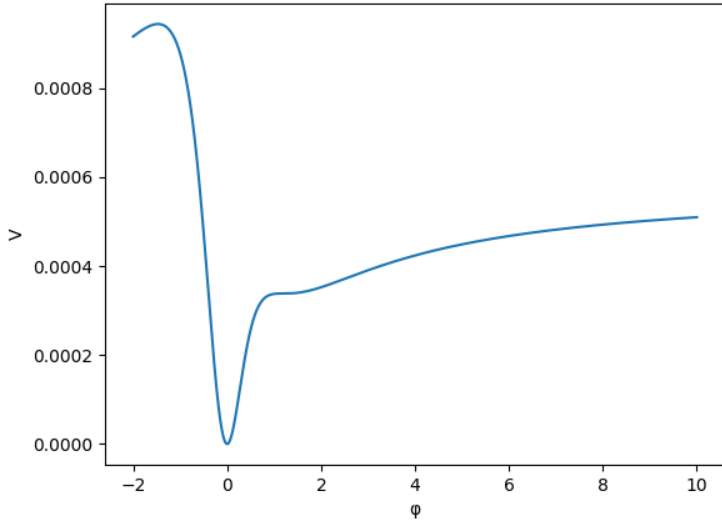


Figure 3.2: In this figure the example potential has been plotted as a function of ϕ . It is clear that the potential has an inflection point.

3.1.4 Example potential

One of the examples of a potential allowing USR inflation is sometimes shown in the form [26, 49]

$$V(x) = V_0 \frac{x^2(6 - 4ax + 3x^2)}{(1 + bx^2)^2}, \quad (3.11)$$

with $x = \frac{\phi}{v}$ and v being just a constant re-scaling factor. The shape of the potential can be seen in figure 3.2. We will be using the same parameters as in [49] i.e. $\frac{V_0}{M_{pl}^4} = 4 \times 10^{-10}$, $\frac{v}{M_{pl}} = \sqrt{0.108}$, $\alpha = 1$ and $\beta = 1.4349$. Now one can find the inflection point of the potential at $V''(x) = 0$. The inflection point using these parameters is located at $\phi_0 = 0.39M_{pl}$. Then by taking the initial value for the field to be $\phi_i = 3.614M_{pl}$ we can numerically calculate using (2.43) and get that the inflation lasts for about 63 e-folds in this model. Which is around the 50-60 that is commonly thought to be needed.

We can calculate the exact evolution of ϵ_H from (2.31). We can see from the behavior of ϵ_H and η_H the background dynamics driven by the potential quite well. In figures 3.3 and 3.4 these parameters have been plotted as a function of e-folds. We can see that during the transition from SR to USR at around 40 e-folds. During the transition ϵ_H rapidly decreases to even smaller values and η_H switches sign and becomes relatively large (around -6).

From the behavior of η_H we easily see that there are two SR regimes separated by a USR regime. During the second SR regime the value of ϵ_H is a few orders of magnitude lower than during the first.

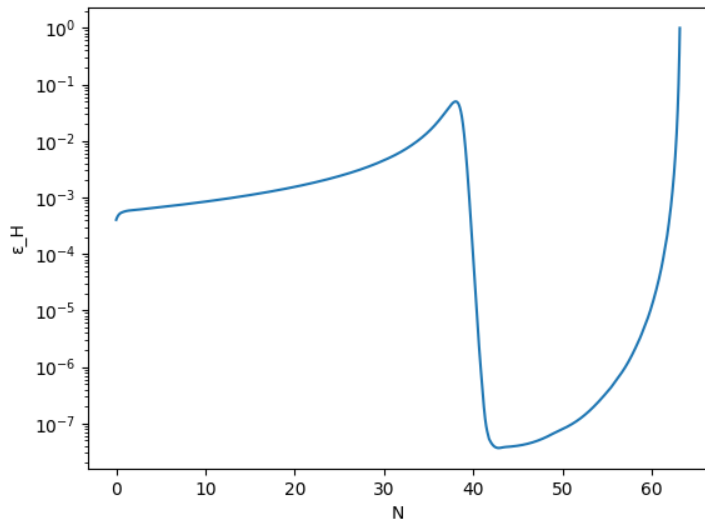


Figure 3.3: This figure shows the evolution of ϵ_H as a function of e-folds.

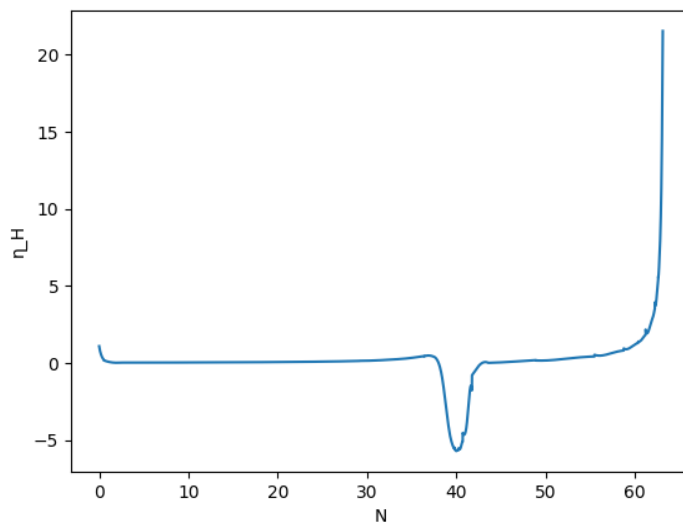


Figure 3.4: This figure shows the evolution of η_H as a function of e-folds.

3.1.5 Punctuated inflation

Punctuated inflation is a inflationary model where there is a brief departure from inflation (SR approximation breaks down as ϵ_H reaches unity) [49]. In such a scenario the interruption of the inflation is inevitably followed by an epoch of USR inflation which then boosts the power spectrum on small scales.

One of the benefits of punctuated inflation is that it can be used to explain the lower power observed at the small multipoles in the CMB data [31]. If the drop is chosen to occur at around the scales corresponding to the Hubble radius today, the resulting power spectrum can improve the fit to a certain extent. Punctuated inflation can come from a potential of the same form as a scenario without the brief departure but with different parameters. Given a potential of similar form to the previous one expressed in terms of $x = \frac{\phi}{v}$ [49]

$$V(x) = V_0 \frac{\alpha x^2 - \beta x^4 + \gamma x^6}{(1 + \delta x^2)^2}, \quad (3.12)$$

one can show that for the following shared parameters $\frac{V_0}{M_{pl}} = 1.3253 \times 10^{-9}$, $\gamma = 1$, $\delta = 1.5092$ and two sets of different parameters $\frac{v}{M_{pl}} = (4.3411, 10)$, $\alpha = (8.522 \times 10^{-2}, 8.53 \times 10^{-2})$ and $\beta = (0.469, 0.458)$ the scenarios will have different properties.

We can get two different evolutions of ϵ_H where in one case it briefly reaches unity before the end of inflation and in the other it does not as seen in figure 3.5. Meaning that one case represents punctuated inflation and the other USR inflation. This illustrates that a scenario cannot be classified to be punctuated inflation or not based on the general form of the potential alone.

3.2 Other inflation models

3.2.1 Higgs inflation

In SM, the only scalar field is the Higgs field. If the Higgs field is coupled to gravity minimally it is not capable of producing a SR inflation model but if it is coupled to gravity non-minimally and extrapolated to high energies this becomes possible.

The action of the SM coupled non-minimally to gravity is [50]

$$S = \int d^4 \sqrt{-g} \left[\frac{1}{2} (M^2 + \xi h^2) g^{\mu\nu} R_{\mu\nu} - \frac{1}{2} g^{\mu\nu} \partial_\mu h \partial_\nu h - V(h) + \mathcal{L}_{SM} \right], \quad (3.13)$$

where $g_{\mu\nu}$ is the metric, M is a mass scale close to Planck mass, h is the radial Higgs field, $R_{\mu\nu}$ is the Ricci tensor, ξ is the non-minimal coupling, $V(h)$ is the potential of the Higgs field ($V(h) = \frac{\lambda}{4} h^4$) and \mathcal{L}_{SM} contains the terms of the Lagrangian from the rest of the SM.

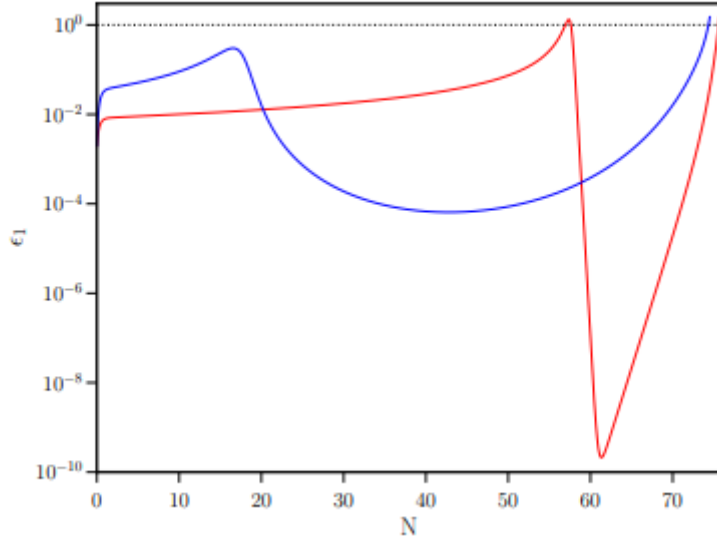


Figure 3.5: In this figure the ϵ_H for both models has been plotted as a function of e-folds. The red line represents punctuated inflation and blue one regular USR. As is seen the red reaches unity for a moment and drops drastically after that. Figure is taken from [49]

By transforming to the Einstein frame we can get rid of the non-minimal coupling [11]

$$g_{\alpha\beta} \rightarrow (1 + \frac{\xi h^2}{M_{pl}^2})^{-1} g_{\alpha\beta} . \quad (3.14)$$

Instead we get a non-minimal kinetic term for the Higgs field. To make it more convenient we will define a new scalar field χ

$$\frac{dh}{d\chi} = \frac{1 + \frac{\xi h^2}{M_{pl}^2}}{\sqrt{1 + \frac{\xi h^2}{M_{pl}^2} + 6 \frac{\xi^2 h^2}{M_{pl}^2}}} . \quad (3.15)$$

This leads to the Einstein frame potential [50]

$$U(\chi) = \frac{V[h(\chi)]}{\left[1 + \frac{\xi h(\chi)^2}{M_{pl}^2}\right]^2} . \quad (3.16)$$

Using this potential Higgs inflation is capable of producing PBHs [50]. Although it is only capable of creating PBHs that have evaporated today to be at most Planck sized relics. Its predictions for the spectral index of primordial scalar perturbations and tensor-to-scalar ratio are in agreement with observations of the CMB [50]. It is the simplest and most minimal way to incorporate inflation into known particle physics.

3.2.2 Hybrid waterfall

Hybrid waterfall inflation model consists of two different fields; the inflaton field ϕ and the auxiliary field χ . In this type of a model the inflaton field is responsible for the expansion and χ is the slowly varying field causing the shift for the potential illustrated in figure 3.6.

The inflation in this model is divided into two phases, the phase where the field is moving along the valley and the waterfall phase. During the first phase χ is considered to be 0 and the SR approximation to be valid. The CMB observations are created during the first phase. When the field value of ϕ falls below a critical value ϕ_c inflation enters the waterfall phase which is illustrated in figure 3.6. As can be seen from the figure the existence of two fields allows for two dimensional motion and after passing the critical point the potential becomes unstable and the small variation of the auxiliary field can cause the fields to roll down the potential.

The essential features can be demonstrated with an example potential [41]

$$V(\phi, \chi) = V_0 + V(\phi) + \frac{1}{2}m^2(\phi)\chi^2 + \frac{1}{4}\lambda\chi^4, \quad (3.17)$$

where

$$m^2(\phi) \equiv g^2\phi^2 - m^2 \equiv g^2(\phi^2 - \phi_c^2). \quad (3.18)$$

In order to have a perturbative quantum theory it has to be that $g \ll 1$ and $\lambda \ll 1$. The inflation is in waterfall when $\phi < \phi_c$.

The equations of motion of the fields are

$$\ddot{\phi} + 3H\dot{\phi} + \frac{\partial V}{\partial \phi} = 0 \quad (3.19)$$

$$\ddot{\chi} + 3H\dot{\chi} + \frac{\partial V}{\partial \chi} = 0. \quad (3.20)$$

During waterfall phase both fields have to be taken into account i.e. one needs to solve the two-field dynamics governed by [17]

$$H^2 = \frac{1}{3M_{pl}^2} \left[\frac{\dot{\phi}^2}{2} + \frac{\dot{\chi}^2}{2} + V(\phi, \chi) \right]. \quad (3.21)$$

Models for waterfall inflation can be categorized based on the length of the waterfall phase in e-folds. The fast waterfall inflation model predicts the formation of very low mass PBH but by having a smaller slope for the potential at the critical point one can increase the number of efolds and the increase of the primordial curvature spectrum [17]. The mild waterfall inflation model for which the waterfall phase lasts for more e-folds induces a larger and broader peak in the scalar power spectrum for modes leaving the Hubble radius during first part of the waterfall phase and produce a significant amount of PBHs [17].

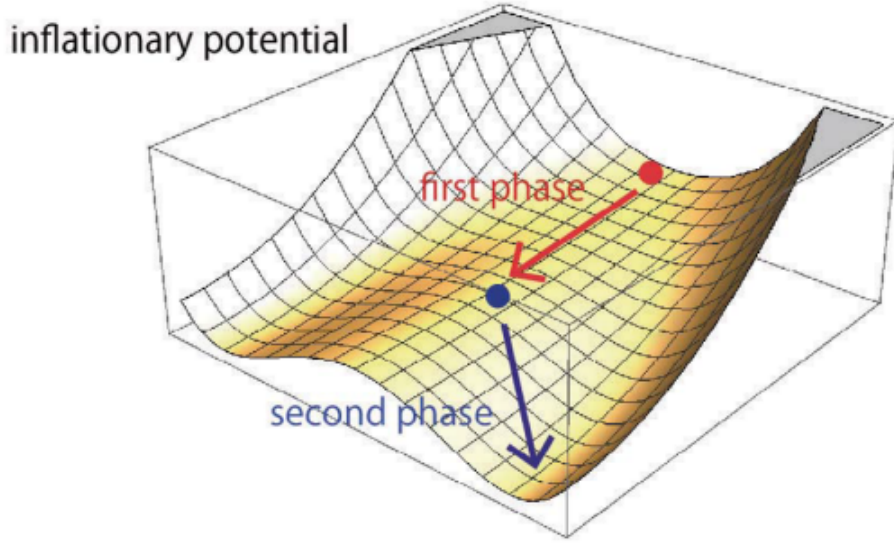


Figure 3.6: Dynamics of the potential of waterfall inflation are illustrated in this figure. Figure taken from [53].

3.2.3 Curvaton

Another example of a two-field model is the curvaton model [53]. In this scenario one of the fields is the inflaton field and is responsible for the exponential expansion of the Universe. The other one is the curvaton field which is responsible for generating the primordial curvature perturbations. In some extensions both fields contribute to the curvature perturbations.

In this manner if we can create a model in which the perturbations on the CMB scales are generated by the inflaton and the small scale ones by the curvaton, then the model is suited for PBH formation and is consistent with the CMB observations. This is one of the benefits compared to single field models.

In the curvaton scenario the power spectrum of the curvaton fluctuations is scale-independent at small scales and has a cut-off at larger scales. During the radiation dominated era after reheating by the decay of the inflaton field, the curvaton field starts to oscillate and the curvaton fluctuations, that are initially isocurvature perturbations, are transformed into adiabatic curvature perturbation. Meaning that the adiabatic curvature perturbation grow in time. Isocurvature perturbation means that the fluctuations of the same wavelength in different species are not spatially in phase while in adiabatic they are. After the decay of the curvaton into radiation the perturbations become constant in time. The components of the perturbations can be seen in figure 3.7 where the inflaton perturbations and the curvaton perturbations for different scales have been plotted. As

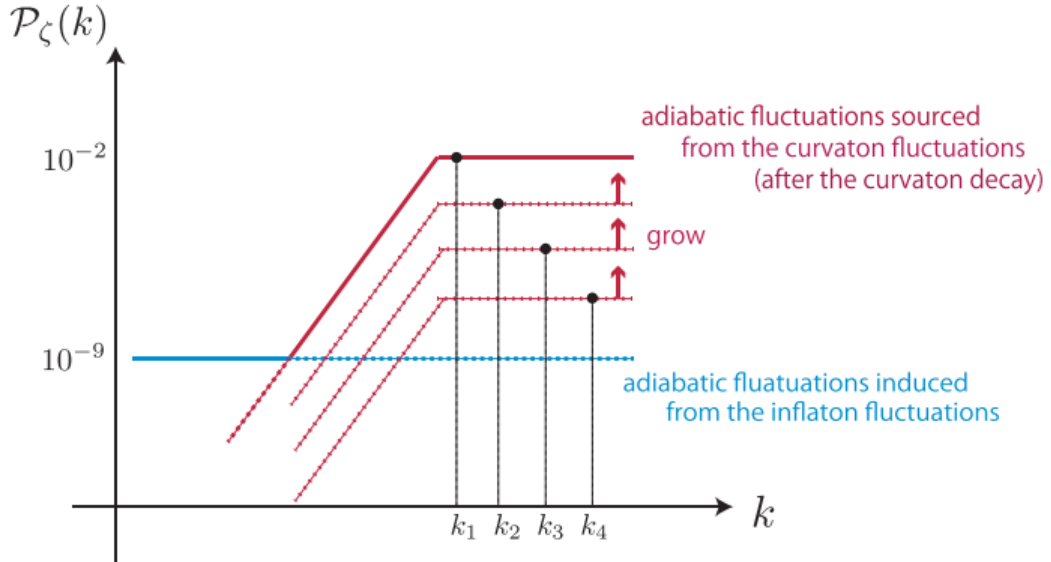


Figure 3.7: Primordial power spectrum in the curvaton scenario where PBH production can be efficient. k_1, k_2, k_3, k_4 correspond to the modes which re-enter at $t = t_1, t_2, t_3, t_4$ with $t_{dec} > t_1 > t_2 > t_3 > t_4$, t_{dec} refers to the time it takes for the curvaton to decay. The adiabatic fluctuation by the inflaton field source the CMB observations while the ones sourced by the curvaton fluctuations are large enough to create PBHs. Figure taken from [53].

can be seen the power spectrum is enhanced by the curvaton perturbations for multiple different scales with different Hubble mass at Hubble re-entry thus the mass spectrum of the formed PBH is broad [53].

4. Formation of PBH and induced gravitational waves from primordial scalar perturbations

In this chapter we cover the production of gravitational waves and PBHs from the primordial scalar perturbations.

4.1 Generation of primordial black holes from re-entry

As mentioned previously, the PBH formation from inflation is due to the primordial perturbations that exit the Hubble radius during inflation and re-enter during the radiation dominated era. Due to the perturbations there are some regions that are overdense which leads to a gravitational collapse after the region becomes causally connected again.

4.1.1 Mass of PBH

The PBHs form with masses that are comparable to the Hubble mass $M_H = \rho V$ at the time of the re-entry [50]

$$M_{PBH} = \gamma M_H = \gamma \rho V = \gamma \frac{4}{3} \pi \rho \left(\frac{1}{H} \right)^3, \quad (4.1)$$

where V is the volume of the causally connected region, $1/H = a/k$ is the Hubble radius, ρ is the total energy density at the time of Hubble re-entry of mode k and γ is an efficiency factor with value $\gamma = 0.2$ in this thesis [50].

During the radiation dominated era the scale factor, density parameter and the Hubble parameter scale as [50]

$$a(t) \propto t^{\frac{1}{2}}, \rho(t) \propto a^{-4} \propto t^{-2}, H(t) = \frac{1}{2t} \propto a^{-2}. \quad (4.2)$$

This means that the wavenumber entering the Hubble radius ($k = aH$) scales as $k \propto a^{-1}$ and the PBH mass scales as

$$M_{PBH} \propto a^2 \propto k^{-2} . \quad (4.3)$$

In order for the PBH to form early enough with masses that could constitute dark matter the wavenumber of re-entry k has to be larger than the pivot scale k_{pivot} denoted as k_* . The number of e-folds of inflation between the Hubble exit of k_* and the Hubble exit k is [50]

$$\Delta N_{k_* k} \equiv N_* - N = \log \frac{a}{a_*} \approx \log \frac{aH}{a_* H_*} = \log \frac{k}{k_*} > 0 . \quad (4.4)$$

This leads to

$$M_{PBH} \propto e^{-2\Delta N_{k_* k}} . \quad (4.5)$$

Approximating that the scaling of the radiation domination era lasts until the matter-radiation equality and inserting values $M_{eq} \approx 6 \times 10^{50} \text{ g}$ for the Hubble mass and $k_{eq} \approx 0.01 \text{ Mpc}^{-1}$ for the wavenumber at the matter-radiation equality in order to normalize the mass of PBHs formed on scale k as [50]

$$M_{PBH} = \gamma \frac{M_{eq}}{25} e^{-2\Delta N_{k_* k}} , \quad (4.6)$$

which can easily be used in inflationary analysis.

4.1.2 Probability distribution of PBH abundance

We assume that the probability distribution for the density perturbations is a Gaussian independent of the model of inflation

$$\mathcal{P}(\delta) = \frac{1}{\sqrt{2\pi\sigma^2}} \exp\left(-\frac{\delta^2}{2\sigma^2}\right) . \quad (4.7)$$

The probability distribution is Gaussian in the case for SR but not necessarily in the case of USR. It is assumed that every region where the primordial perturbation \mathcal{R} (or δ) exceeds the threshold value \mathcal{R}_c (or δ_c) collapses into a black hole. We can then evaluate the fraction of the Universe collapsing into PBH of mass M

$$\beta(M) \equiv \frac{\rho_{PBH}}{\rho} = 2 \int_{\delta_c}^{\infty} d\delta \mathcal{P}(\delta) \simeq \text{erfc}\left(\frac{\delta_c}{\sqrt{2\sigma^2}}\right) , \quad (4.8)$$

where erfc is the complementary error function defined as

$$\text{erfc } z \equiv 1 - \text{erf } z = \frac{2}{\sqrt{\pi}} \int_z^{\infty} e^{-t^2} dt . \quad (4.9)$$

In the limit $\sigma \ll \delta_c$ one finds

$$\beta(M) = \frac{\sigma}{\sqrt{2\pi}\delta_c} e^{-\frac{\delta_c^2}{2\sigma^2}} , \quad (4.10)$$

where the variance σ of the density perturbations is related to the power spectrum by $\langle \delta^2 \rangle = \sigma^2 \approx \mathcal{P}_\delta(k_r)$ where k_r is the wavenumber re-entering inside the Hubble radius at time t_r . A more accurate treatment of the relationship between the variance and the power spectrum is done with a suitable window function to smooth the density contrast δ on the scale of PBH formation [13]

$$\sigma^2 = \int_0^\infty \widetilde{W}^2(kR) \mathcal{P}_\delta d \ln k , \quad (4.11)$$

where \widetilde{W} is the Fourier transform of a real space window function. The choice of a window function can change the value of σ^2 by an order of magnitude [8]. For the purposes of this thesis we will use an approximation for the window function of a step function in k-space.

The relation between the density contrast δ and the primordial curvature perturbation during the radiation dominated era is $\delta = \frac{4}{9} \left(\frac{k}{aH} \right)^2 \mathcal{R}$ [13]. At the Hubble entry ($k=aH$) they are related by the factor $\frac{4}{9}$. So the equation for the fraction of PBH becomes [22, 50]

$$\beta \simeq \operatorname{erfc} \left(\frac{9\delta_c}{4\sqrt{2\mathcal{P}_\mathcal{R}}} \right) \simeq \frac{\sqrt{2\mathcal{P}_\mathcal{R}}}{\sqrt{\pi}\mathcal{R}_c} e^{-\frac{\mathcal{R}_c^2}{2\mathcal{P}_\mathcal{R}}} . \quad (4.12)$$

There are many studies trying to evaluate \mathcal{R}_c . One of the analytical approximations for a given equation of state parameter is given by [17]

$$\mathcal{R}_c = \frac{1}{3} \ln \frac{3(\chi_a - \sin \chi_a \cos \chi_a)}{2 \sin^3 \chi_a} , \quad (4.13)$$

with $\chi_a = \frac{\pi\sqrt{\omega}}{(1+3\omega)}$. Which for $\omega = \frac{1}{3}$ leads to $\mathcal{R}_c \simeq 0.086$. Different values are obtained using different methods but in general it seems that \mathcal{R}_c lies between $0.07 \lesssim \mathcal{R}_c \lesssim 1.3$ [50].

4.2 Gravitational waves induced by primordial perturbations

In linear perturbation theory, tensor and scalar perturbations are decoupled and evolve separately but at second order this is not the case. Gravitational waves induced by the primordial scalar perturbations are a consequence of the coupling of the scalar perturbations at second order. In the scales of PBH formation the enhancement of the power spectrum during USR might cause the induced gravitational waves to have a more significant contribution when compared to the primordial tensor perturbations.

4.2.1 The metric

The perturbed metric can be decomposed as [7]

$$g_{\alpha\beta} = \bar{g}_{\alpha\beta} + \delta g_{\alpha\beta} + \delta^2 g_{\alpha\beta} , \quad (4.14)$$

where $\bar{g}_{\alpha\beta}$ is the FLRW background, $\delta g_{\alpha\beta}$ has purely scalar degrees of freedom and $\delta^2 g_{\alpha\beta}$ has in general scalar, vector and tensor modes induced by $\delta g_{\alpha\beta}$. However, as we are only interested in the induced tensor modes we drop any scalar and vector modes at second order. We then write the perturbed metric as [53]

$$ds^2 = a^2(\eta) \left\{ -(1 + \Phi)d\eta^2 + \left[(1 - 2\Psi)\delta_{ij} + \frac{1}{2}h_{ij} \right] dx^i dx^j \right\} , \quad (4.15)$$

where Φ and Ψ are the Bardeen potentials that describe scalar perturbations at first order [58], for which in the absence of anisotropic stress $\Phi = \Psi$, and h_{ij} represents the induced second order tensor perturbations. Due to the traceless and transverse nature of the tensor perturbations $\partial^i h_{ij} = 0$ and $h_i^i = 0$.

4.2.2 Induced gravitational waves

The Fourier transform of h_{ij} can be written as [7]

$$h_{ij}(\mathbf{x}, \eta) = \frac{1}{(2\pi)^{3/2}} \int d^3k e^{i\mathbf{k}\cdot\mathbf{x}} \left[h^+(\mathbf{k}, \eta) q_{ij}^+(\mathbf{k}) + h^\times(\mathbf{k}, \eta) q_{ij}^\times(\mathbf{k}) \right] , \quad (4.16)$$

where q_{ij}^+ and q_{ij}^\times denote the polarization tensors that have non-zero components in the plane perpendicular to the direction of the propagation and are expressed in terms of orthonormal basis vectors \mathbf{e} and $\bar{\mathbf{e}}$ orthogonal to \mathbf{k}

$$q_{ij}^+ = \frac{1}{\sqrt{2}} [e_i(\mathbf{k})e_j(\mathbf{k}) - \bar{e}_i(\mathbf{k})\bar{e}_j(\mathbf{k})] \quad (4.17)$$

$$q_{ij}^\times = \frac{1}{\sqrt{2}} [e_i(\mathbf{k})\bar{e}_j(\mathbf{k}) + \bar{e}_i(\mathbf{k})e_j(\mathbf{k})] . \quad (4.18)$$

Orthonormality leads to the normalization condition: $q_{ij}^\lambda(\mathbf{k})q^{\lambda',ij} = \delta^{\lambda\lambda'}$, where λ and λ' can be either $+$ or \times .

The modes we are interested in re-enter the Hubble radius during the radiation dominated era. The equation of motion of the Fourier modes can be derived using the Einstein equations perturbed to second order that describes the induced tensor perturbation h_{ij} and the Bardeen equation that is a differential equation that describes the scalar perturbations when $\Phi = \Psi$ [36]. During radiation domination in Fourier space the amplitude of the tensor mode, for each polarization, follow the equation [7]

$$\frac{d^2 h(\vec{k}, \tau)}{d\tau^2} + \frac{2}{\tau} \frac{dh(\vec{k}, \tau)}{d\tau} + k^2 h(\vec{k}, \tau) = \mathcal{S}(\vec{k}, \tau) , \quad (4.19)$$

where the source term \mathcal{S} is [22]

$$\begin{aligned} \mathcal{S} = & \int \frac{d^3 \tilde{k}}{(2\pi)^{3/2}} \tilde{k}^2 \left[1 - \left(\frac{\vec{k} \cdot \vec{\tilde{k}}}{k \tilde{k}} \right)^2 \right] \left\{ 12\Phi(\vec{k} - \vec{\tilde{k}}, \tau)\Phi(\vec{\tilde{k}}, \tau) \right. \\ & \left. + 8 \left[\tau\Phi(\vec{k} - \vec{\tilde{k}}, \tau) + \frac{\tau^2}{2} \frac{d\Phi(\vec{k} - \vec{\tilde{k}}, \tau)}{d\tau} \right] \frac{d\Phi(\vec{\tilde{k}}, \tau)}{d\tau} \right\} , \end{aligned} \quad (4.20)$$

where the Bardeen potential $\Phi = 2\mathcal{R}/3$ satisfies the equation [22]

$$\frac{d^2\Phi}{d\tau^2} + \frac{4}{\tau} \frac{d\Phi}{d\tau} + \frac{1}{3} k^2 \Phi = 0 \quad (4.21)$$

Solving the first equation using the Green function method allows us to relate the current relative energy density of the gravitational waves with the power spectrum as [22]

$$\Omega_{GW}(k, \eta_0) = 10\mathcal{P}_{\mathcal{R}}^2 a_{eq} , \quad (4.22)$$

where a_{eq} is the value of the scale factor at the matter radiation equality and the current scale factor $a_0 = 1$, $a_{eq} = \frac{a_0}{3.1 \times 10^4 \Omega_M h^2}$ [25], $h \equiv H_0/(100 \text{km/s/Mpc})$.

4.2.3 Relation to PBH mass

The production of the gravitational waves by the second order effect happens at the same time as PBH formation i.e. when the modes re-enter the Hubble radius. Once the gravitational waves have been produced they propagate freely during the later epochs of the Universe due to their low interaction rate. The frequency of the gravitational waves produced is comparable to the Hubble mass at the time and given that the mass of PBH is also proportional to the Hubble mass, we can relate the PBH mass to the frequency of the gravitational waves at the present time as [53]

$$f_{GW} \simeq 10^{-9} \text{Hz} \left(\frac{M_{PBH}}{30 M_{\odot}} \right)^{-\frac{1}{2}} . \quad (4.23)$$

From this we can see that the production of solar mass PBH generate ultra-low frequency GWs in the nHz band.

5. Primordial black holes as a dark matter candidate

Due to the detection of binary black hole pairs by LIGO, Virgo and KAGRA, the idea that primordial black holes could constitute most of the dark matter in the Universe has acquired more momentum. The colliding pairs can also be astronomical black holes instead of primordial ones due to their mass and merging rate [51] but if one can find a black hole with mass less than Chandrasekhar limit that would be direct evidence for the existence of PBHs.

The benefit of the idea that PBHs constitute all of dark matter is that it requires no new physics beyond the SM to exist in addition to inflation as a production mechanism for the PBHs.

The frequently used parameter for parametrizing the fraction of PBH as dark matter is

$$f \equiv \frac{\rho_{PBH}}{\rho_{DM}} , \quad (5.1)$$

where ρ_{DM} is the energy density of dark matter and $f = 1$ means that all of dark matter is made out of PBHs.

5.1 Mass scales

Different models for PBH production predict a wide range of possible masses for PBH. There exist multiple observational constraints for massive black holes but there currently is a sizable mass window where $f = 1$ is a possibility. It is between $10^{17} - 10^{22}$ g or in terms of solar mass $10^{-16} - 10^{-12} M_{\odot}$ and is called the asteroid mass window [13]. The masses of the PBH created by the gravitational collapse caused by the primordial density perturbations are model dependent and the constraints can be used to constrain possible inflation models and to suggest new models. The most significant observational constraints that we will consider are shown in figure 5.1.

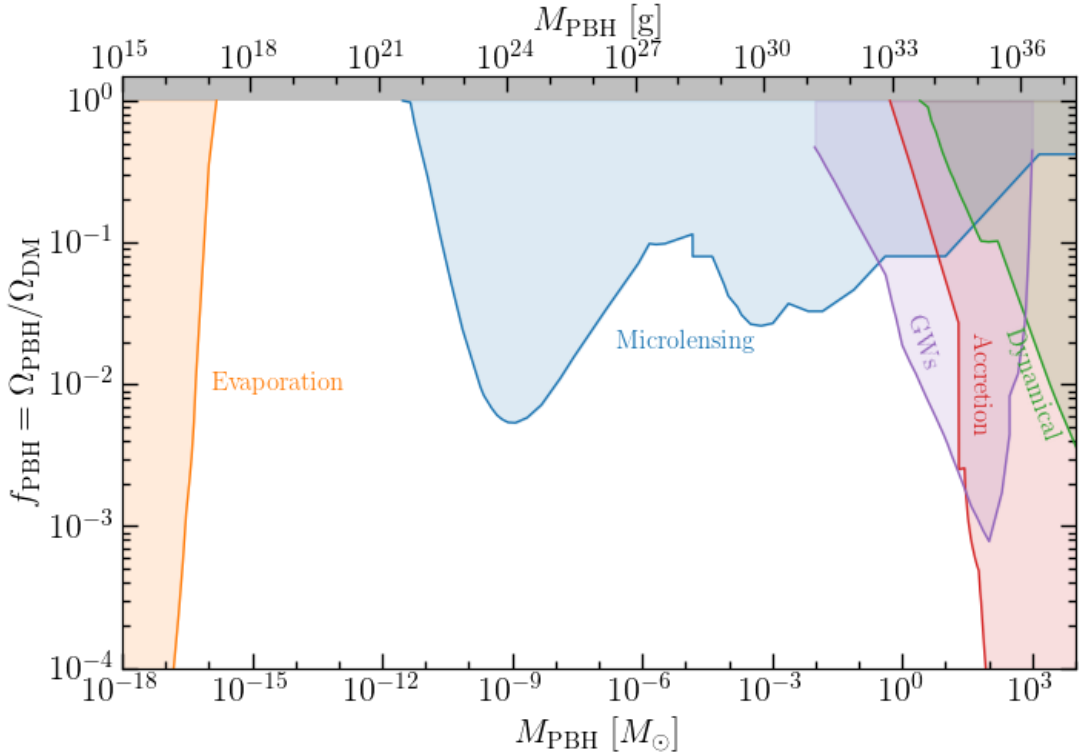


Figure 5.1: All current major limits on different PBH masses is presented in this figure. Figure made with PBH bounds given in [28].

5.2 Planck mass relics

Due to the Hawking radiation masses below around 10^{15} g have evaporated by the present day but when the PBH comes close to evaporating and the mass becomes comparable to Planck mass, it is possible that the semi-classical physics used to derive Hawking radiation fail and the evaporation halts at the Planck scale. In this case the evaporated PBH could leave behind a stable relic that could constitute all of dark matter.

Because of the possibility that the evaporation of PBH could change the elements of baryogenesis, the PBH must form at early times with mass less than 10^6 g. Evaporating ones larger than this would dominate the total energy density before evaporation in which case the final cosmological photon-to-baryon ratio is determined by the baryon asymmetry of the emissions of the PBH [14]. The mass 10^6 g using (4.6) corresponds to $\Delta N \gtrsim 49$, meaning that the perturbations must leave the Hubble radius near the end of inflation.

The energy density at matter-radiation equality is approximately

$$\Omega_{rel} = \frac{M_{relic}}{M_{PBH}} \frac{k}{k_{eq}} \beta_k \approx \frac{M_{rel}}{M_{pl}} e^{3\Delta N - 123}, \quad (5.2)$$

for values $M_{relic} = M_{pl}$ and $\Delta N = 50$ this is of the order of unity for $\beta \sim e^{-30}$ which corresponds to $\mathcal{P}_R \approx 10^{-2} \mathcal{R}_c^2 \sim 10^{-4} - 10^{-2}$. If the spectrum can be enhanced to this

range at the end of inflation, it is possible for the relics to constitute all of dark matter.

This scenario could be considered a nightmare dark matter scenario as it is possible that the relics can't be detected with any known technology. Although there have been suggestions that the relics could carry a random electric charge and could be detected that way [38]. It has also been suggested that the relics gain a significant velocity (of the order $\approx 10^{-1}c$) from the decay process which would rule them out as a cold dark matter candidate [35]. The current observations seem to favor cold, meaning non-relativistic, dark matter.

5.3 Observational limitations

There exist several different types of observational limitations for the mass spectrum of possible existing PBH and on the primordial power spectrum. We will go through the most important ones in this section utilizing [28].

5.3.1 Microlensing constraints

Microlensing is a phenomenon that occurs if a sufficiently compact object (with mass in the range $5 \times 10^{-10} M_\odot \lesssim M \lesssim 10 M_\odot$) crosses the line of sight of a distant luminous object. The light of the source will be gravitationally focused and thus enhanced. The duration of the microlensing event is proportional to $M^{\frac{1}{2}}$, so the range of masses constrained by a microlensing survey depends on its cadence i.e. the interval between observations. For a object with mass $10^{-6} M_\odot$ the time is a few hours and for a $10 M_\odot$ object the timescale is of the order of months.

The EROS-2 survey of the Magellanic clouds found the constraint $f_{PBH} \lesssim 0.1$ for the mass range $10^{-6} - 1 M_\odot$ [56]. The constraint weakens above $M \approx M_\odot$ reaching $f_{PBH} \lesssim 1$ for $M \approx 30 M_\odot$. Additionally a MACHO collaboration search for long duration events (longer than 150 days) places similar constraints for masses $1 M_\odot \lesssim M \lesssim 30 M_\odot$ [3]. In this case the uncertainties in density and velocity distribution of the PBH have a significant impact of the microlensing constraints and the constraints change if the compact objects were to be clustered.

Tighter constraints have been obtained using OGLE microlensing survey of the Galactic bulge for $M \sim 10^{-3} M_\odot$ with $f_{PBH} \lesssim 10^{-2}$. The constraints lessen to $f_{PBH} \lesssim 0.1$ for masses $M \lesssim 10^{-5} M_\odot$ and $10^{-2} M_\odot$ [45, 47].

A one night high cadence scan by the Hyper-Supreme Cam (HSC) on Subaru telescope of M31 improved constraints in the mass range $5 \times 10^{-10} M_\odot \lesssim M \lesssim 10^{-8} M_\odot$ with $f_{PBH} \lesssim 10^{-2}$ and ruled out $f_{PBH} = 1$ for mass range $10^{-12} M_\odot \lesssim M \lesssim 10^{-6} M_\odot$ [19, 48]. Once accounting for the finite source and wave optics effects, the constraints are weaker

than initially thought. Finite source meaning that once the apparent size in the sky of the lensing object is comparable to the apparent size of the object lensed the lensing is only effective on the part of the surface of the lensed star and not the entire surface making the enhancement of luminosity too small to be detectable. The Schwarzschild radius of a PBH with mass $M \lesssim 10^{-10} M_\odot$ is comparable to, or less than, the wavelength of the light observed. So the wave optics effects (interference and diffraction effects) that reduce the amplification have to be taken into account [55].

5.3.2 Accretion

The high energy radiation emitted by the gas accretion onto PBHs can be detected. This has been demonstrated by the recent images taken by the Event Horizon Telescope of two supermassive black holes. The constraints can be divided into ones from the time of the formation of the CMB and the ones from the present day.

The present day constraints come from the accretion of interstellar gas onto PBH with mass $M \gtrsim 10 M_\odot$. Such an accretion leads to observable x-ray and radio wave emission [24]. Comparing the prediction of numerical simulations and the observational data gained from the Chandra and VLA Galactic centre survey lead to a constraint of $f \lesssim 10^{-3}$ for $M \sim (30 - 100) M_\odot$ [42]. From gas heating in dwarf galaxies we get a constraint $f \lesssim 10^{-4}$ for $M \sim 10^3 M_\odot$ which weakens to $f \lesssim 1$ for the masses $M \sim M_\odot$ and $M \sim 10^7 M_\odot$ [40].

The constraints from accretion happening at the formation of the CMB are based on the modification of the recombination history which affects the anisotropies and the spectrum of the CMB.

Assuming the accretion disk is spherical the constraints are $f \lesssim 1$ for $M \gtrsim$ few M_\odot . The constraints are much tighter for larger masses, $f \lesssim 10^{-4}$ for $M \gtrsim 10^2 M_\odot$ and $f \lesssim 3 \times 10^{-9}$ for $M \sim 10^4 M_\odot$ [54].

Accretion is not expected to be significant for PBH with an initial mass much below $10 M_\odot$. The PBH below that mass and above the mass where Hawking radiation becomes significant are considered to have around a constant mass.

5.3.3 Discreteness effects or dynamical constraints

Discreteness effects or sometimes called dynamical constraints are caused by very massive PBHs not being distributed as a smooth field on small scales. As two-body interactions equalize the kinetic energies of different mass populations in a system that is made of stars and more massive compact object (e.g. PBHs), the stars would gain energy causing their distribution to expand. Ultra-faint dwarf galaxies are sensitive to this effect and it has been found by the observed sizes of such systems place constraints of $f \lesssim 0.002 - 0.004$

for $M \sim 10^4 M_\odot$ weakening to $f \lesssim 1$ for $M \sim 10 M_\odot$ [12].

Another system of interest are wide binaries as the energy of the system is increased by multiple encounters with compact objects. These encounters could lead to a disruption of the system. The separation distribution of wide binaries can be then used to constrain the abundance of compact objects. Though a radial measurement is required to confirm that the binaries are genuine and not spurious binaries. Using 25 wide binaries from [5] that spend least time in the galactic disk so that they are not as often effected by encounters with stars it was found that $f \lesssim 0.1$ for $M \gtrsim 70 M_\odot$ with the limit weakening to $f \lesssim 1$ for $M \sim 3 M_\odot$ [44].

5.3.4 Evaporation constraints

The emission of the black hole will increase at lower mass, so the emission of black holes of mass $M_* < M \lesssim 10^{17} g$ is sufficient that their abundance can be constrained using their evaporation products. The lower limit M_* refers to the mass for which the PBH would have already completely evaporated.

The effect of black holes evaporating during the time of BBN on the abundances of light elements formed during it also places restrictions on those masses. The abundance of black holes that evaporate before the BBN ($M \lesssim 10^{10} g$) is difficult to constrain using any observations. There are certain signals that could limit these [53]. Production of the lightest supersymmetric particles, gravitinos and neutralinos by the evaporation of PBH (assuming they exist) in the early Universe could constrain part of that range. Neutralinos and gravitinos set the constraint for $M < 10^9 g$ and the constraint set by the lightest supersymmetric particles is dependant on its mass ($M < 10^{11} (m_{LSP}/100 \text{GeV})^{-1} g$) [14].

5.3.5 Constraints from the power spectrum

The constraints for the power spectrum come from two sources, the CMB and the scalar-induced gravitational waves.

The CMB constraint comes from the lack of spectral distortions in the CMB. One of the types of spectral distortion is the μ -type. It is a thermal distortion from the black body distribution characterized by non-zero chemical potential μ . COBE FIRAS instrument confirmed that the CMB photons follow a black body distribution and theoretically it has been found that the damping of large amplitude density perturbations during certain redshifts cause energy injections and a deviation from the black body spectrum [13]. Due to the lack of the detection of a cosmic- μ distortion the constraint for the power spectrum becomes $\mathcal{P}_R \lesssim 10^{-4}$ in the range $k \sim 10^4 \text{ Mpc}^{-1}$ in which the smallest constrained mass is $\sim 10^4 M_\odot$ [13].

The gravitational wave based constraint comes from pulsar timing arrays (PTA). Pulsars are rapidly rotating neutron stars that emit beams of radio waves. The possible change in the pulse arrival times of certain pulsars (millisecond pulsars) and can be used to probe for low-frequency gravitational waves. The stochastic background of scalar induced gravitational waves created by the scale corresponding to a Hubble mass $M_H \sim 1M_\odot$ has a frequency that can be probed with PTAs. Although these constraints are inflation model dependent, some of the constraints found are $f < 1$ for $10^{-2}M_\odot \lesssim M \lesssim 1M_\odot$ and with the data from NANOGrav, $f < 1$ for $M \approx 0.1M_\odot$ and $f < 10^{-6}$ for $0.002M_\odot < M < 0.4M_\odot$ [15].

5.3.6 Gravitational wave constraints

The gravitational wave constraints are currently based on the observations of the gravitational wave observatories LIGO and Virgo of merging compact objects.

The standard calculation of the mergers assumes that PBHs form binary pairs in the very early Universe and that many remain undisturbed until today. Estimating the disruption rate is numerically challenging and is often model dependent (though it is normally agreed upon that disruption is very important when $f \simeq 1$ but can be neglected for $f \lesssim 10^{-2}$). Given no clustering and no disruption of the binaries the merging rate should be several orders of magnitude higher than measured by LIGO-Virgo and that places the constraint of the order $f \lesssim 10^{-3}$ for $10M_\odot \lesssim M \lesssim 300M_\odot$ [4, 33]. A dedicated LIGO-Virgo search for sub-Solar mass mergers places a constraint of the order $f \lesssim 10^{-1}$ down to $M \sim 0.2M_\odot$ [2]. LIGO and Virgo are most sensitive in the $1 - 10^2M_\odot$ region and while they can detect the sub solar range the microlensing constraints are stronger on these scales.

There exists tight constraints on the existence of PBH of mass range $M \sim 10^{13-15}g$ from the induced gravitational waves detectable by LIGO. Such masses should have evaporated from Hawking radiation but if this process is not realized in reality, the PBH would be stable and viable as dark matter.

5.3.7 Future constraints for the asteroid mass range

Possible methods for constraining the asteroid mass range ($10^{17}g < M < 10^{22}g$) have been suggested. The asteroid mass range and the suggested constraints are shown in figure 5.2.

The most stringent constraint would come from the measurement of the lensing parallax of gamma ray bursts [32]. Meaning measuring the relative brightness of a source measured by multiple telescopes at large spatial separations. If the spatial separation is large enough the lensing caused by the PBH on the gamma ray burst will be detected by the two detectors as different lensing magnifications.

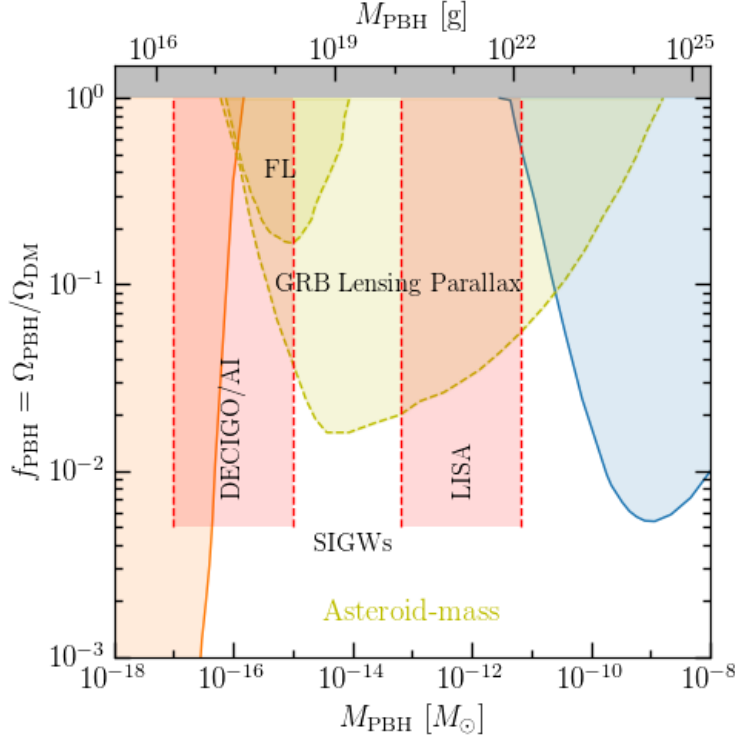


Figure 5.2: Possible future constraints for the asteroid-mass range are shown in this figure. Figure made with PBH bounds given in [28].

It has been proposed that compact object of this mass could be probed by femtolensing of gamma-ray bursts, especially through oscillatory features in photon spectrum of the gamma-ray bursts. The basic assumption of femtolensing is that a gamma-ray emitted by a point-like source is split into two rays by the lens each of which is delayed with respect to the unlensed ray by a time shift. Assuming the two rays cannot be resolved in space and time they will interfere and produce characteristic fringes in the spectrum. However most gamma-ray bursts are too wide to be modelled as point sources and wave-optics effects need to be taken into account. Currently there are no constraints from femtolensing but a small subset of gamma-ray bursts with fast variability have small sizes and are suitable for femtolensing [40]. This could be used to probe the mass range $10^{17}g \lesssim M \lesssim 10^{19}$.

The gravitational wave detectors LISA and DECIGO could in theory detect the scalar-induced gravitational waves created during inflation for some of the mass range as shown in figure 5.2.

5.4 Future gravitational wave detectors

5.4.1 LISA

LISA (Laser Interferometer Space Antenna) is a collaboration between ESA and NASA and is set to launch in the early 2030s [6].

It is planned to consist of three drag-free spacecraft with a distance of around 2.5×10^6 km between them in a equilateral triangle configuration in the same orbit as the Earth. Some of the aims are the detection of compact object binaries and to study their evolution and formation, study of the origin of massive black holes and to explore the fundamental nature of gravity and black holes [6].

LISA is optimized to detect gravitational waves in the 10 mHz region and in general would be able to detect the range of 0.1 mHz-1 Hz (scales $k = 6.456 \times 10^{10} \text{Mpc}^{-1}$ to $k = 6.456 \times 10^{15} \text{Mpc}^{-1}$). It could be then used to probe the induced stochastic gravitational waves induced by the re-entry of these scales corresponding to PBH masses of around $M \simeq 10^{-12} M_\odot$ [9].

5.4.2 DECIGO

DECIGO (Deci-hertz Interferometer Gravitational Wave Observatory) [34] is a planned Japanese space mission in order to detect gravitational waves of the frequency band 0.1 Hz and 10 Hz (scales $k = 6.456 \times 10^{14} \text{Mpc}^{-1}$ to $k = 6.456 \times 10^{16} \text{Mpc}^{-1}$). This closes the gap between LISA 0.1 mHz-1 Hz) and LIGO (10 Hz- 10 kHz [43]).

It is planned to consist of four clusters of observatories put into a heliocentric orbit in such a way that two of the cluster are placed at the same position in the orbit.

The aim is for example to detect the gravitational waves produced during the inflationary period and gauge the acceleration of the expansion of the Universe through neutron star binaries. The mission is hoped to launch after a pathfinder mission B-DECIGO that is to be launched in the 2030s to demonstrate and test the technologies necessary for DECIGO.

6. Conclusion

The detection of even a single PBH would have significant impact on our understanding of the Universe. Since PBH require a large amplitude of density perturbations to be generated during inflation, it would tell us that some special conditions e.g. a period ofUSR is required in order to produce them. The detection could also explain part or the entirety of dark matter.

Even the non-detection of PBH is of interest due to the constraints placed on the primordial power spectrum on the widest range of scales. These constraints could then be used to rule out possible inflation scenarios and design new ones.

The future detection of primordial gravitational waves would give for the first time a direct probe into the time before the birth of the CMB. This would be of a great utility in understanding the first moments of our Universe.

We have gone over some of the inflation scenarios where PBH production is possible in an interesting quantity. The future for the verification or falsification of these models is bright as there are different possible future observations that could be used for the detection of the produced PBH and gravitational waves. The future searches are sure to answer important questions independent of the possible outcomes of the search.

Bibliography

- [1] B. P. Abbott et al. “Observation of Gravitational Waves from a Binary Black Hole Merger”. In: *Physical Review Letters* 116.6 (Feb. 2016). arXiv: [1602.03837v1](https://arxiv.org/abs/1602.03837v1) [gr-qc].
- [2] B. P. Abbott et al. “Search for Subsolar Mass Ultracompact Binaries in Advanced LIGO’s Second Observing Run”. In: *Physical Review Letters* 123.16 (Oct. 2019). arXiv: [1904.08976v3](https://arxiv.org/abs/1904.08976v3) [astro-ph.CO].
- [3] C. Alcock et al. “MACHO Project Limits on Black Hole Dark Matter in the 1–30 M_{\odot}] Range”. In: *The Astrophysical Journal* 550.2 (Apr. 2001), pp. L169–L172. arXiv: [astro-ph/0011506v1](https://arxiv.org/abs/astro-ph/0011506v1).
- [4] Yacine Ali-Haïmoud, Ely D. Kovetz, and Marc Kamionkowski. “Merger rate of primordial black-hole binaries”. In: *Physical Review D* 96.12 (Dec. 2017). arXiv: [1709.06576v2](https://arxiv.org/abs/1709.06576v2) [astro-ph.CO].
- [5] Christine Allen and Miguel A. Monroy-Rodríguez. “AN IMPROVED CATALOG OF HALO WIDE BINARY CANDIDATES”. In: *The Astrophysical Journal* 790.2 (July 2014), p. 158. arXiv: [1406.5164v1](https://arxiv.org/abs/1406.5164v1) [astro-ph.SR].
- [6] Pau Amaro-Seoane et al. *Laser Interferometer Space Antenna*. 2017. arXiv: [1702.00786v3](https://arxiv.org/abs/1702.00786v3) [astro-ph.IM].
- [7] Kishore N. Ananda, Chris Clarkson, and David Wands. “Cosmological gravitational wave background from primordial density perturbations”. In: *Physical Review D* 75.12 (June 2007). arXiv: [gr-qc/0612013v1](https://arxiv.org/abs/gr-qc/0612013v1).
- [8] Kenta Ando, Keisuke Inomata, and Masahiro Kawasaki. “Primordial black holes and uncertainties in the choice of the window function”. In: *Phys. Rev. D* 97 (10 May 2018), p. 103528. arXiv: [1802.06393v2](https://arxiv.org/abs/1802.06393v2) [astro-ph.CO].
- [9] N. Bartolo et al. “Testing primordial black holes as dark matter with LISA”. In: *Physical Review D* 99.10 (May 2019). arXiv: [1810.12224v3](https://arxiv.org/abs/1810.12224v3) [astro-ph.CO].

- [10] Nicola Bellomo et al. “Primordial black holes as dark matter: converting constraints from monochromatic to extended mass distributions”. In: *Journal of Cosmology and Astroparticle Physics* 2018.01 (Jan. 2018), pp. 004–004. arXiv: [1709.07467v2 \[astro-ph.CO\]](https://arxiv.org/abs/1709.07467v2).
- [11] Fedor Bezrukov and Mikhail Shaposhnikov. “The Standard Model Higgs boson as the inflaton”. In: *Physics Letters B* 659.3 (Jan. 2008), pp. 703–706. arXiv: [0710.3755v2 \[hep-th\]](https://arxiv.org/abs/0710.3755v2).
- [12] Timothy D. Brandt. “CONSTRAINTS ON MACHO DARK MATTER FROM COMPACT STELLAR SYSTEMS IN ULTRA-FAINT DWARF GALAXIES”. In: *The Astrophysical Journal* 824.2 (June 2016), p. L31. arXiv: [1605.03665v2 \[astro-ph.CO\]](https://arxiv.org/abs/1605.03665v2).
- [13] Christian T. Byrnes and Philippa S. Cole. *Lecture notes on inflation and primordial black holes*. 2021. arXiv: [2112.05716 \[astro-ph.CO\]](https://arxiv.org/abs/2112.05716).
- [14] B. J. Carr et al. “New cosmological constraints on primordial black holes”. In: *Physical Review D* 81.10 (May 2010). arXiv: [0912.5297v2 \[astro-ph.CO\]](https://arxiv.org/abs/0912.5297v2).
- [15] Zu-Cheng Chen, Chen Yuan, and Qing-Guo Huang. “Pulsar Timing Array Constraints on Primordial Black Holes with NANOGrav 11-Year Dataset”. In: *Physical Review Letters* 124.25 (June 2020). arXiv: [1910.12239v4 \[astro-ph.CO\]](https://arxiv.org/abs/1910.12239v4).
- [16] Nelson Christensen. “Stochastic gravitational wave backgrounds”. In: *Reports on Progress in Physics* 82.1 (Nov. 2018), p. 016903. arXiv: [1811.08797v1 \[gr-qc\]](https://arxiv.org/abs/1811.08797v1).
- [17] Sébastien Clesse and Juan García-Bellido. “Massive primordial black holes from hybrid inflation as dark matter and the seeds of galaxies”. In: *Physical Review D* 92.2 (July 2015). arXiv: [1501.07565v1 \[astro-ph.CO\]](https://arxiv.org/abs/1501.07565v1).
- [18] Philippa S. Cole. *Small-scale probes of the early universe, Ph.D. thesis, Sussex U.* 2021. eprint: <http://sro.sussex.ac.uk/id/eprint/96490/>.
- [19] Djuna Croon et al. “Subaru-HSC through a different lens: Microlensing by extended dark matter structures”. In: *Physical Review D* 102.8 (Oct. 2020). arXiv: [2007.12697v1 \[astro-ph.CO\]](https://arxiv.org/abs/2007.12697v1).
- [20] Heling Deng. “Primordial black hole formation by vacuum bubbles. Part II”. In: *Journal of Cosmology and Astroparticle Physics* 2020.09 (Sept. 2020), pp. 023–023. arXiv: [2006.11907v2 \[astro-ph.CO\]](https://arxiv.org/abs/2006.11907v2).
- [21] Heling Deng, Jaume Garriga, and Alexander Vilenkin. “Primordial black hole and wormhole formation by domain walls”. In: *Journal of Cosmology and Astroparticle Physics* 2017.04 (Apr. 2017), pp. 050–050. arXiv: [1612.03753v4 \[gr-qc\]](https://arxiv.org/abs/1612.03753v4).

- [22] Haoran Di and Yungui Gong. “Primordial black holes and second order gravitational waves from ultra-slow-roll inflation”. In: *Journal of Cosmology and Astroparticle Physics* 2018.07 (July 2018), pp. 007–007. arXiv: [1707.09578v3 \[astro-ph.CO\]](https://arxiv.org/abs/1707.09578v3).
- [23] Konstantinos Dimopoulos. “Ultra slow-roll inflation demystified”. In: *Physics Letters B* 775 (Dec. 2017), pp. 262–265. arXiv: [1707.05644v3 \[hep-ph\]](https://arxiv.org/abs/1707.05644v3).
- [24] Daniele Gaggero et al. “Searching for Primordial Black Holes in the Radio and X-Ray Sky”. In: *Physical Review Letters* 118.24 (June 2017). arXiv: [1612.00457v2 \[astro-ph.HE\]](https://arxiv.org/abs/1612.00457v2).
- [25] Juan Garcia-Bellido. *Astrophysics and Cosmology*. 2000. arXiv: [hep-ph/0004188v1](https://arxiv.org/abs/hep-ph/0004188v1).
- [26] Juan García-Bellido and Ester Ruiz Morales. “Primordial black holes from single field models of inflation”. In: *Physics of the Dark Universe* 18 (Dec. 2017), pp. 47–54. arXiv: [1702.03901v6 \[astro-ph.CO\]](https://arxiv.org/abs/1702.03901v6).
- [27] Jaume Garriga and Alexander Vilenkin. “Black holes from nucleating strings”. In: *Physical Review D* 47.8 (Apr. 1993), pp. 3265–3274. arXiv: [hep-ph/9208212v1](https://arxiv.org/abs/hep-ph/9208212v1).
- [28] Anne M Green and Bradley J Kavanagh. “Primordial black holes as a dark matter candidate”. In: *Journal of Physics G: Nuclear and Particle Physics* 48.4 (Feb. 2021), p. 043001. arXiv: [2007.10722v3 \[astro-ph.CO\]](https://arxiv.org/abs/2007.10722v3).
- [29] Guzzetti et al. In: *La Rivista del Nuovo Cimento* 39.9 (Aug. 2016), 399â495. ISSN: 0393697X, 0393697X. arXiv: [1605.01615v3 \[astro-ph.CO\]](https://arxiv.org/abs/1605.01615v3).
- [30] Stephen Hawking. “Gravitationally Collapsed Objects of Very Low Mass”. In: *Monthly Notices of the Royal Astronomical Society* 152.1 (Apr. 1971), pp. 75–78. ISSN: 0035-8711. DOI: [10.1093/mnras/152.1.75](https://doi.org/10.1093/mnras/152.1.75).
- [31] Rajeev Kumar Jain et al. “Punctuated inflation and the low CMB multipoles”. In: *Journal of Cosmology and Astroparticle Physics* 2009.01 (Jan. 2009), pp. 009–009. arXiv: [0809.3915v2 \[astro-ph\]](https://arxiv.org/abs/0809.3915v2).
- [32] Sunghoon Jung and TaeHun Kim. “Gamma-ray burst lensing parallax: Closing the primordial black hole dark matter mass window”. In: *Physical Review Research* 2.1 (Feb. 2020). arXiv: [1908.00078v2 \[astro-ph.CO\]](https://arxiv.org/abs/1908.00078v2).
- [33] Bradley J. Kavanagh, Daniele Gaggero, and Gianfranco Bertone. “Merger rate of a subdominant population of primordial black holes”. In: *Physical Review D* 98.2 (July 2018). arXiv: [1805.09034v3 \[astro-ph.CO\]](https://arxiv.org/abs/1805.09034v3).
- [34] Seiji Kawamura et al. *Current status of space gravitational wave antenna DECIGO and B-DECIGO*. 2020. arXiv: [2006.13545v1 \[gr-qc\]](https://arxiv.org/abs/2006.13545v1).
- [35] Samuel Kováčik. *Hawking-Radiation Recoil of Microscopic Black Holes*. 2021. arXiv: [2102.06517v2 \[gr-qc\]](https://arxiv.org/abs/2102.06517v2).

- [36] Hannu Kurki-Suonio. *Cosmological perturbation theory lecture notes, Spring*. 2022. eprint: <http://www.courses.physics.helsinki.fi/teor/cpt/CosPer.pdf>.
- [37] Hannu Kurki-Suonio. *Cosmology 2 lecture notes, Fall*. 2021. eprint: http://www.courses.physics.helsinki.fi/teor/cosmology/Cosm_II.pdf.
- [38] Benjamin V. Lehmann et al. “Direct detection of primordial black hole relics as dark matter”. In: *Journal of Cosmology and Astroparticle Physics* 2019.10 (Oct. 2019), pp. 046–046. arXiv: [1906.06348v2 \[hep-ph\]](https://arxiv.org/abs/1906.06348v2).
- [39] Andrew R. Liddle, Paul Parsons, and John D. Barrow. “Formalizing the slow-roll approximation in inflation”. In: *Physical Review D* 50.12 (Dec. 1994), pp. 7222–7232. arXiv: [astro-ph/9408015v1](https://arxiv.org/abs/astro-ph/9408015v1).
- [40] Philip Lu et al. “Constraining Primordial Black Holes with Dwarf Galaxy Heating”. In: *The Astrophysical Journal Letters* 908.2 (Feb. 2021), p. L23. arXiv: [2007.02213v2 \[astro-ph.CO\]](https://arxiv.org/abs/2007.02213v2).
- [41] David H Lyth. “The hybrid inflation waterfall and the primordial curvature perturbation”. In: *Journal of Cosmology and Astroparticle Physics* 2012.05 (May 2012), pp. 022–022. arXiv: [1201.4312v4 \[astro-ph.CO\]](https://arxiv.org/abs/1201.4312v4).
- [42] Julien Manshanden et al. “Multi-wavelength astronomical searches for primordial black holes”. In: *Journal of Cosmology and Astroparticle Physics* 2019.06 (June 2019), pp. 026–026. arXiv: [1812.07967v2 \[astro-ph.HE\]](https://arxiv.org/abs/1812.07967v2).
- [43] D. V. Martynov et al. “Sensitivity of the Advanced LIGO detectors at the beginning of gravitational wave astronomy”. In: *Physical Review D* 93.11 (June 2016). arXiv: [1604.00439v3 \[astro-ph.IM\]](https://arxiv.org/abs/1604.00439v3).
- [44] Miguel A. Monroy-Rodríguez and Christine Allen. “THE END OF THE MACHO ERA, REVISITED: NEW LIMITS ON MACHO MASSES FROM HALO WIDE BINARIES”. In: *The Astrophysical Journal* 790.2 (July 2014), p. 159. arXiv: [1406.5169v1 \[astro-ph.GA\]](https://arxiv.org/abs/1406.5169v1).
- [45] Przemek Mróz et al. “No large population of unbound or wide-orbit Jupiter-mass planets”. In: *Nature* 548.7666 (July 2017), pp. 183–186. DOI: [10.1038/nature23276](https://doi.org/10.1038/nature23276).
- [46] Y. Akrami N. Aghanim et al. “iPlanck/i2018 results”. In: *Astronomy & Astrophysics* 641 (Sept. 2020), A10. arXiv: [1807.06209v4 \[astro-ph.CO\]](https://arxiv.org/abs/1807.06209v4).
- [47] Hiroko Niikura et al. “Constraints on Earth-mass primordial black holes from OGLE 5-year microlensing events”. In: *Physical Review D* 99.8 (Apr. 2019). arXiv: [1901.07120v2 \[astro-ph.CO\]](https://arxiv.org/abs/1901.07120v2).

[48] Hiroko Niikura et al. “Microlensing constraints on primordial black holes with Subaru/HSC Andromeda observations”. In: *Nature Astronomy* 3.6 (Apr. 2019), pp. 524–534. arXiv: [1701.02151v3 \[astro-ph.CO\]](https://arxiv.org/abs/1701.02151v3).

[49] H. V. Ragavendra et al. “Primordial black holes and secondary gravitational waves from ultraslow roll and punctuated inflation”. In: *Physical Review D* 103.8 (Apr. 2021). arXiv: [2008.12202v3 \[astro-ph.CO\]](https://arxiv.org/abs/2008.12202v3).

[50] Syksy Räsänen and Eemeli Tomberg. “Planck scale black hole dark matter from Higgs inflation”. In: *Journal of Cosmology and Astroparticle Physics* 2019.01 (Jan. 2019), pp. 038–038. arXiv: [1810.12608v2 \[astro-ph.CO\]](https://arxiv.org/abs/1810.12608v2).

[51] Carl L. Rodriguez et al. “The Observed Rate of Binary Black Hole Mergers can be Entirely Explained by Globular Clusters”. In: *Research Notes of the AAS* 5.1 (Jan. 2021), p. 19. arXiv: [2101.07793v2 \[astro-ph.HE\]](https://arxiv.org/abs/2101.07793v2).

[52] Alberto Salvio. “Hearing Higgs with gravitational wave detectors”. In: *Journal of Cosmology and Astroparticle Physics* 2021.06 (June 2021), p. 040. arXiv: [2104.12783v2 \[hep-ph\]](https://arxiv.org/abs/2104.12783v2).

[53] Misao Sasaki et al. “Primordial black holes—perspectives in gravitational wave astronomy”. In: *Classical and Quantum Gravity* 35.6 (Feb. 2018), p. 063001. arXiv: [1801.05235v1 \[astro-ph.CO\]](https://arxiv.org/abs/1801.05235v1).

[54] Pasquale D. Serpico et al. “Cosmic microwave background bounds on primordial black holes including dark matter halo accretion”. In: *Physical Review Research* 2.2 (May 2020). arXiv: [2002.10771v2 \[astro-ph.CO\]](https://arxiv.org/abs/2002.10771v2).

[55] Sunao Sugiyama, Toshiki Kurita, and Masahiro Takada. “On the wave optics effect on primordial black hole constraints from optical microlensing search”. In: *Monthly Notices of the Royal Astronomical Society* 493.3 (Feb. 2020), pp. 3632–3641. arXiv: [1905.06066v3 \[astro-ph.CO\]](https://arxiv.org/abs/1905.06066v3).

[56] P. Tisserand et al. “Limits on the Macho content of the Galactic Halo from the EROS-2 Survey of the Magellanic Clouds”. In: *Astronomy & Astrophysics* 469.2 (Apr. 2007), pp. 387–404. arXiv: [astro-ph/0607207v2](https://arxiv.org/abs/astro-ph/0607207v2).

[57] M. Tristram et al. “Improved limits on the tensor-to-scalar ratio using BICEP and *Planck* data”. In: *Phys. Rev. D* 105 (8 Apr. 2022), p. 083524. arXiv: [2112.07961v2 \[astro-ph.CO\]](https://arxiv.org/abs/2112.07961v2).

[58] Claes Uggla and John Wainwright. “Cosmological perturbation theory revisited”. In: *Classical and Quantum Gravity* 28.17 (Aug. 2011), p. 175017. arXiv: [1102.5039v2 \[gr-qc\]](https://arxiv.org/abs/1102.5039v2).